Leclerc, M. – Grono, E. – Hardy, K. – Lim, T. S. – Troitzsch, U. – Brink, F. – Clark, G. R. – Tanudirjo, D. A. – Azis, N. – Reepmeyer, C.

Automated analysis of pottery by QEM-EDS: a case study from Mansiri, Sulawesi

aus / from

Journal of Global Archaeology, 2023: pp. 50–93

DOI: https://doi.org/10.34780/b92n-4tna

Herausgebende Institution / Publisher:
Deutsches Archäologisches Institut

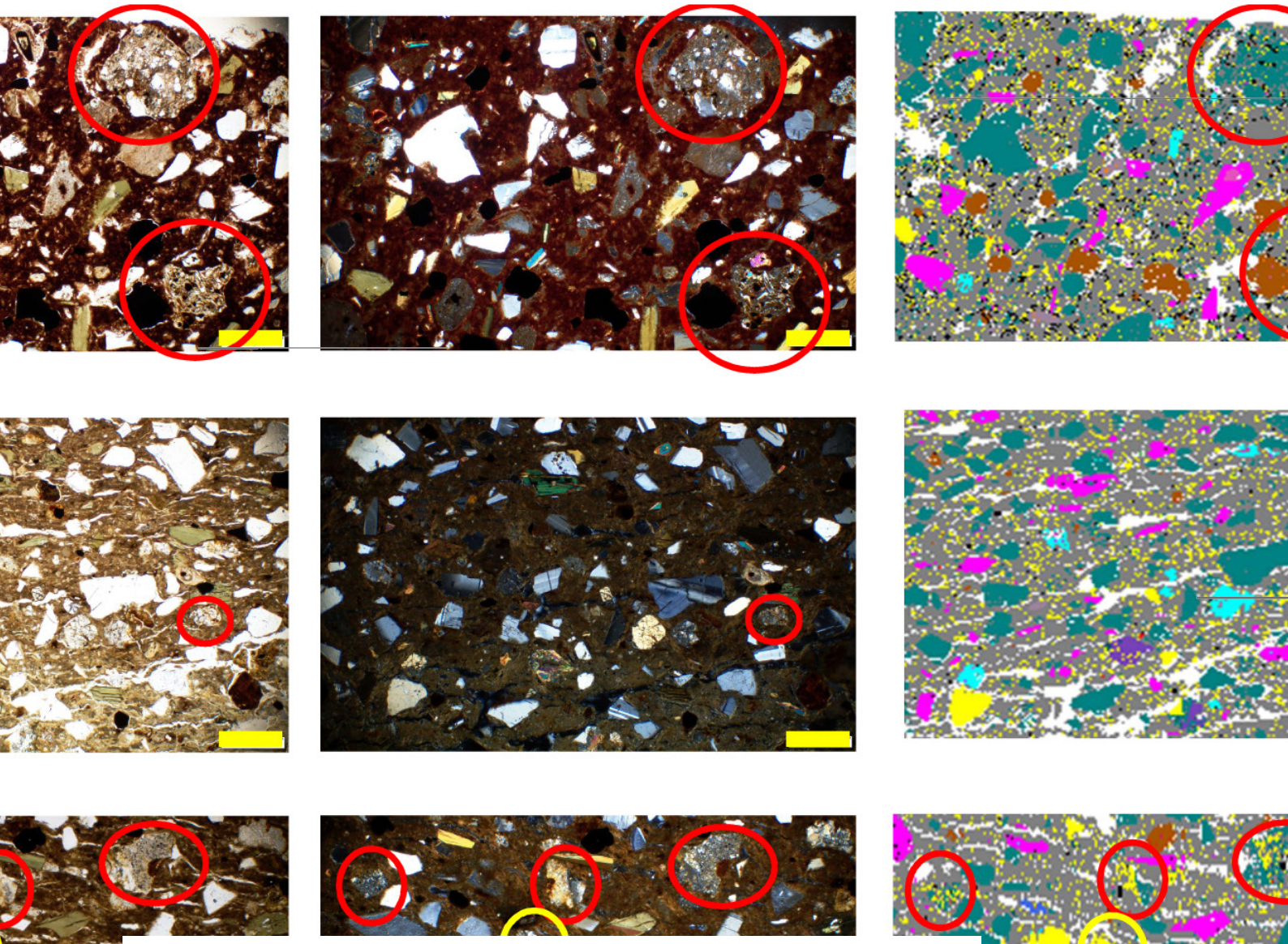

AUTOMATED ANALYSIS OF POTTERY BY QEM-EDS

A case study from Mansiri, Sulawesi

M. Leclerc – K. Hardy – E. Grono – T. Siang Lim – U. Troitzsch – F. Brink – G. Clark – D. Tanudirjo – N. Azis – C. Reepmeyer

The analysis of raw materials and manufacturing techniques is central to the investigation of pottery assemblages. While various analytical techniques exist, petrography generally remains the go-to method to analyse the fabric of pottery. It combines relatively cheap and simple sample preparation protocol with the ability to yield very detailed information related to provenance and manufacturing technique. Here, we test the utility of performing QEM-EDS on archaeological pottery from the Mansiri site, Sulawesi, to complement petrographic observations. We identify the main non-plastic inclusions as plagioclase, quartz, calcic amphibole, iron oxides and volcanic rock fragments, consistent with the pottery being made locally. Quantitative analysis of inclusion size and direction suggests that the non-plastic inclusions were not manually added, and that in contrast to other Neolithic Sulawesi sites, coiling with beating/paddle and anvil was used to manufacture the pots.

KEYWORDS

Pottery, Automated Petrographic Analysis, QEMSCAN, Quantitative Mineral Analysis, Sulawesi, Island Southeast Asia

MATHIEU LECLERC – KRISTINE HARDY – ELLE GRONO – TSE SIANG LIM – ULRIKE TROITZSCH – FRANK BRINK – GEOFFREY CLARK – DAUD TANUDIRJO – NAZRULLAH AZIS – CHRISTIAN REEPMEYER

Automated analysis of pottery by QEM-EDS

A case study from Mansiri, Sulawesi

1. INTRODUCTION

1 The analysis of raw materials used to produce prehistoric pottery represents a key component of archaeological research. Whilst pottery is generally composed of two main components (clay matrix and mineralogical/organic inclusions), the variability of these constituents and the almost infinite combinations of ingredients and actions during the manufacturing process make the analysis of pottery fabrics and technology a fairly complex field of research. Traditional approaches to obtain quantitative (or semi-quantitative) data rely on visual estimation using manual counts, comparison charts and/or micrometre/eyepiece graticules (Reedy et al. 2014). While these estimations are valuable, their reproducibility and accuracy are dependent on the analyst's experience and they can be time-consuming. In recent years, image analysis involving the segmentation of components based on their visual properties has emerged as a reliable technique to acquire quantitative values from thin sections of pottery.

2 Petrography has been traditionally employed to understand mineralogical temper additions, however, in recent decades various geochemical techniques have been applied more regularly to understand raw material provenance and manufacturing processes (e.g., Dickinson 2006, Gaffney et al. 2015, Leclerc et al. 2019). Petrographic analysis of ceramics involves, among other things, the identification, classification and quantification of inclusions in the clay matrix (Quinn 2013). These inclusions are called 'temper' if they were manually added by potters to the ceramic paste, and 'non-plastic inclusions' if they were naturally present in the clay. The analysis of inclusions is helpful in various aspects of pottery production, such as identifying curation of raw materials and providing scientific evidence of transportation or local production of ceramics. Key textural characteristics observable by petrography, such as size, directionality and structural arrangements of mineral grains also reveal some of the technological decisions taken by prehistoric potters (Quinn 2013, Reedy 2008). The quantitative measurement of these attributes can contribute to a better understanding of pottery manufacturing processes.

3 When used conjointly with classic petrographic analysis, image analysis from optical microscopy and SEM back-scattered images can be used to develop strategies for automated petrographic analysis (e.g., Aprile et al. 2014, Aprile et al. 2019, Dal Sasso et al. 2014, Eramo et al. 2014, Reedy et al. 2014). In this paper, we intend to test another possible avenue for automating mineralogical inclusion analysis using the combination

of petrography, QEM-EDS (Quantitative Evaluation of Minerals using Energy Dispersive Spectroscopy) using the QEMSCAN© technology, XRD (X-Ray Diffraction analysis) and SEM-EDS (scanning electron microscopy–energy dispersive X-ray analysis). QEM-EDS was originally developed in the late 1970s by the Commonwealth Scientific and Industrial Research Organisation (CSIRO) for rapid, quantitative and operator-independent acquisition of X-ray spectra for mineralogical analysis (Butcher et al. 2000; Pirrie et al. 2004). Amongst QEM-EDS main advantages is the ability to undertake systematic mineralogical mapping of the whole sample area (Šegvić et al. 2014), which can significantly improve the textural and compositional characterisation of the sample (e.g., Edwards et al. 2017, Ward et al. 2017). Results are cross-examined by XRD and petrography to improve the accuracy of mineral identification by QEM-EDS. In our study, we also employed SEM-EDS to assist in differentiating amphibole from pyroxene grains.

4 QEM-EDS provides an output very similar to digital image analysis but the mineralogical maps produced are based on the chemical composition of the constituents, as opposed to their visual properties. Here, we test the applicability of QEM-EDS for pottery analysis, by assessing if it is able to: a) identify mineral grains accurately in pottery samples; b) assess fabric types; and c) undertake a textural analysis of the fabrics in order to identify the manufacturing technique based on quantitative data for mineralogical grain parameters (abundances, size distribution and directionality). This article details a case study illustrating the potential of this approach by using pottery sherds from the Neolithic site of Mansiri, Sulawesi, Indonesia (Azis et al. 2018).

5 QEM-EDS has been successfully applied in various contexts, such as the mining industry (Goodall et al. 2005, Goodall 2008, Gottlieb et al. 2000), geophysics (Martin et al. 2008), forensic science (Pirrie et al. 2004, Pirrie et al. 2009) and soil micromorphology (Edwards et al. 2017, Prossor et al. 2022, Mason et al. 2022, Ward et al. 2017). Its applicability for archaeological purposes, however, remains to be fully tested, even though a few pilot studies have already used QEM-EDS to analyse pottery and identified "enormous potential" (Knappett et al. 2011; see also Šegvić et al. 2016). Despite promising potential, QEM-EDS's limitations are well documented and particularly significant for pottery analysis. QEM-EDS outputs are at times ambiguous in identifying minerals with similar chemical compositions, mineral polymorphs or amorphous material (Knappett et al. 2011, Pirrie et al. 2004). Minerals in solid solution or metastable phases, such as those produced by firing at high temperature, frequently have non-uniform spectra and are difficult to define (Šegvić et al. 2014). In this paper, we explore whether these challenges are insurmountable obstacles or if they can be overcome.

6 In addition to automated mineral identification, the quantitative data produced by QEM-EDS will also inform on the pottery manufacturing process. The degree of sorting can be related to depositional environments and/or is indicative of manipulations of the raw material by the potter (Quinn 2013). The orientation and alignment of the grains can also be correlated with the primary forming technique (Carr 1990, Rye 1981). How physical force is applied to plastic clay will affect the alignment of the components. For example, pinching and/or moulding, two manufacturing techniques based on similar actions and movements, can often be differentiated from coiling (Berg 2009, Carr 1990, Thér 2016). In theory, coil manufacturing would result in less aligned grains compared to other techniques when cutting perpendicularly to the coils (Berg 2009: Fig. 5, Thér 2016: Fig. 5). While these issues are commonly investigated by thin section analysis (Whitbread 1996a, Whitbread 1996b), X-ray radiography (Berg 2011, Berg – Ambers 2016, Middleton 2005, Rye 1977), SEM (Courty – Roux 1995; Felicissimo et al. 2010) and more recently micro-CT (Kozatsas et al. 2018, Sanger 2016), the article will detail how QEM-EDS can contribute to this field of study.

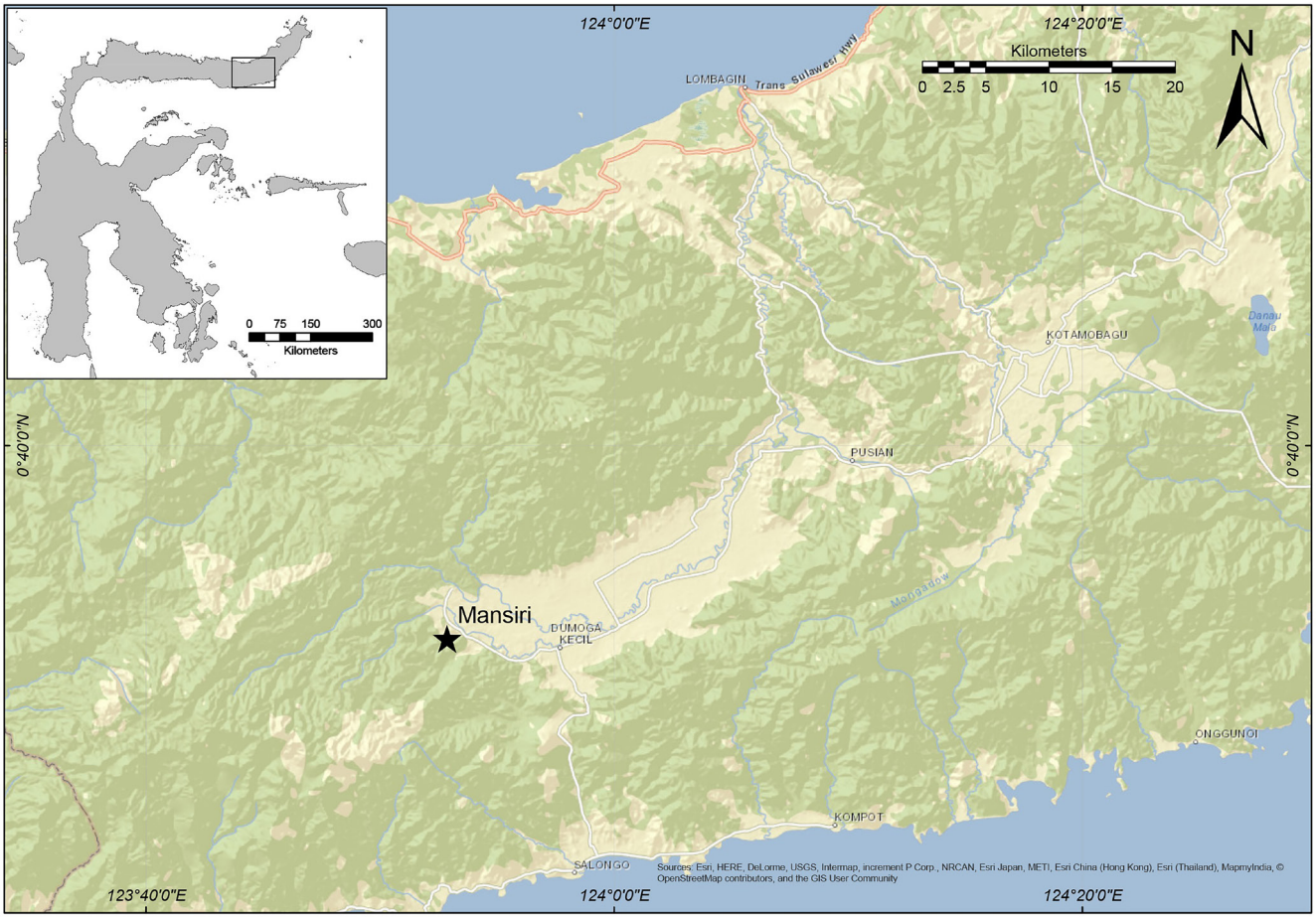

Fig. 1: Location of Mansiri on Sulawesi.

2. MATERIALS AND METHODS

2.1. Mansiri

7 Mansiri (N0°32'42", E123°52'3") is a Neolithic site located in the Bogani Nani Wartabone National Park, Bolaang Mongondow Regency of Northern Sulawesi, approximately 50 km west of Kotamobagu City (Fig. 1) (Azis et al. 2018). Situated in an upland region of North Sulawesi, the site is most likely associated with a main inland river system in a similar settlement pattern as in neighbouring regions, such as the Karama Valley in Western Sulawesi (Anggraeni et al. 2014). The Mansiri site is located at 273 m asl at the western end of the Dumoga Valley in the foothills of the Central Mountain range. The site experiences an equatorial climate and used to be covered by tropical rainforest. Details about its geological setting are provided in Fig. 2 and Supplementary A.

8 Preliminary investigations at the Mansiri site have revealed substantial Neolithic deposits, containing thousands of ceramic fragments, including pieces which resemble the spectacular decorated pottery of the Lapita culture in the Pacific (Azis et al. 2018). While the small amount of decorated pottery at Mansiri parallels some of the techniques and designs identified in Lapita and Island Southeast Asia (ISEA) assemblages, Mansiri also contains vessel forms that have not been identified in any Lapita assemblage. The initial and tentative dating of Mansiri indicates initial occupation around 3300–2700 cal BP, which is later than the emergence of Lapita pottery in the East. The ceramics might represent two-way movement between ISEA and the West Pacific after the initial occurrence of Lapita pottery in the Bismarck Archipelago (Denham et al. 2013, Specht et al. 2014).

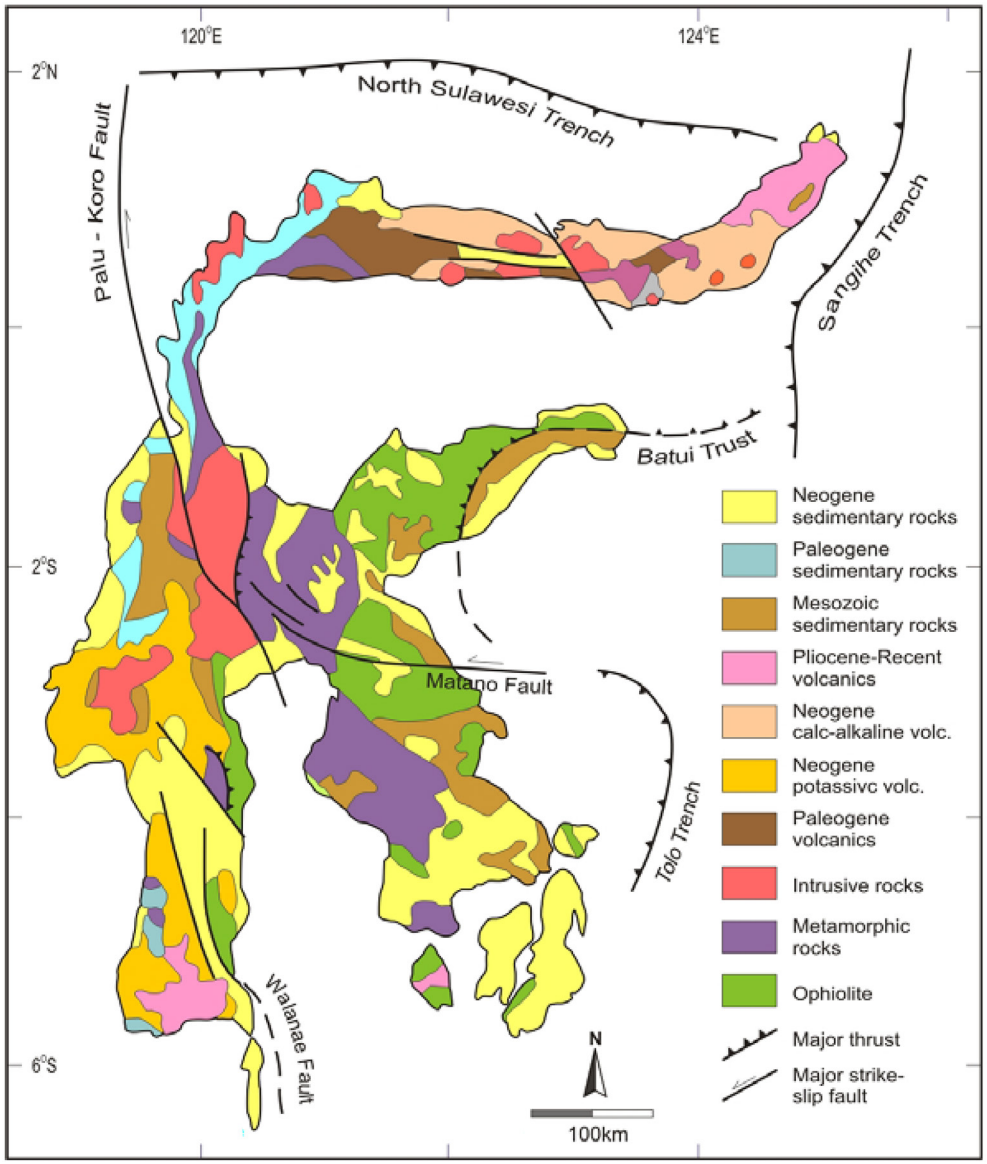

Fig. 2: Simplified geological map of Sulawesi (modified from van Leeuwen and Pieters 2011).

9 Pottery from Mansiri was selected for this project because of the apparent homogeneity of its assemblage observed by macroscopic analysis. Indeed, a quantitative approach is particularly suitable for the analysis of homogeneous ceramic assemblages because it allows the detection of minor differences that may be overlooked by visual analysis alone (Quinn 2013: 102–105). In light of this, a sample of ten pottery sherds from the Mansiri site were selected for this case study. The pottery samples included red painted and slipped wall sherds and three rim sherds.

2.2. Sample preparation & analysis

10 The ten pottery sherds were prepared into thin sections at the Research School of Earth Sciences of The Australian National University (ANU) following standard procedures for ceramic petrography (Sherds and orientation of the sections on Fig. 3; Details about preparation in Supplementary A).

2.2.1 QEM-EDS

11 The QEM-EDS analyses in this study were performed using a FEI Quanta QEMSCAN® system at the Centre for Advanced Microscopy (CAM) at the ANU. It utilises an automated scanning electron microscope which has been equipped with multiple energy-dispersive X-ray spectrometers to optimise X-ray count rate. As the electron

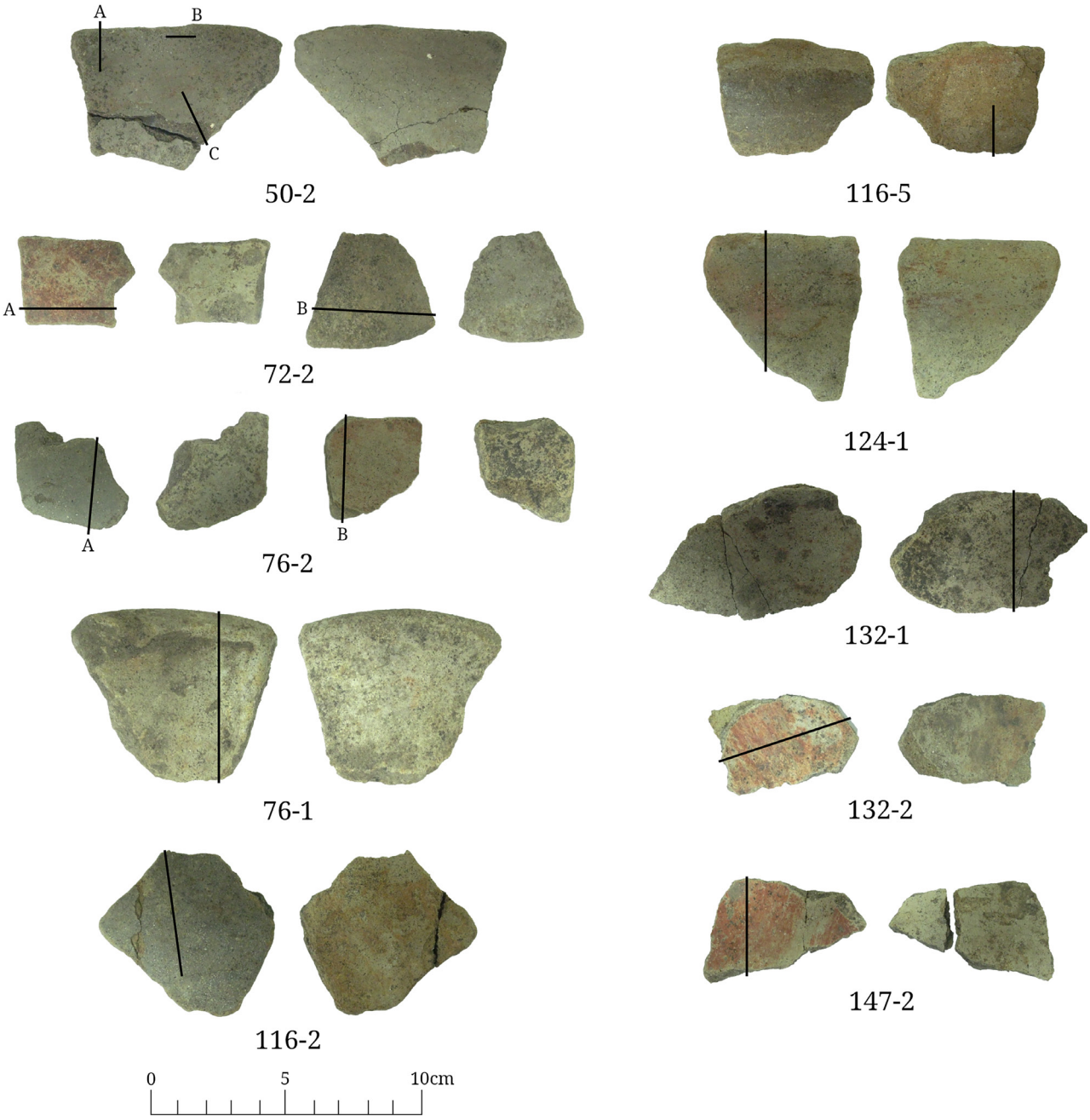

Fig. 3: Sherds from Mansiri and the locations of the cuts for thin sections.

beam is scanned across the surface in a series of digitised steps, a full EDS spectrum (typically containing 2000–4000 counts) is collected at each point (pixel), resulting in a full spectrum X-ray map. Data was collected with QEMSCAN in field image scan mode, 15kV accelerating voltage, 10 nA probe current and a step size of 20 µm. The X-ray acquisition process is optimised by avoiding collection of spectral data on non-mineral regions by utilising the backscattered electron (BSE) signal at each pixel. For regions yielding BSE intensities below a pre-set intensity, typical of resin filled pore spaces or organic material, no EDS data is collected. ThermoFisher iMeasure software was used for data acquisition and ThermoFisher iDiscover and FEI iNanomin were used for frame stitching and final mineral identification.

12 Mineral identification and modal fractions were performed using ThermoFisher iNanomin. This process involves comparison of the unknown spectrum at each pixel to known mineral reference spectra held within the Mineral Reference Editor (MRE). A successful mineral classification is assigned to a pixel only if a spectral match of better than a pre-set fitting value has been achieved. Failure in classifying pixels can either be due to a mineral being absent from the MRE or sometimes due to

pixels being located on the boundary between two different mineral grains where a mixed spectrum is obtained. Mineral identifications derived from SEM, petrographic and XRD analysis were integrated in the MRE to ensure the accuracy of automated identifications.

13 Size and directionality of the grains were measured for the most common minerals. Diameter (minimum Feret distance), area and angle were measured using automated particle detection ('Analyze Particles') in Fuji ImageJ software (Schindelin et al. 2012). Krumbein Phi was calculated from the $-\text{Log}_2$ minimum Feret. Only particles at least 5000 μm^2 (12.5 pixels) were used to calculate the angle, as larger particles are more sensitive to directional pressures.

14 To calculate the angle of the crystals relative to the sherd wall the images were subset into areas where the angle of the wall was relatively constant (Supplementary B). The mean angle between the wall and the x axis was obtained from three different measurements. The minerals were converted to ellipses and the major ellipse axis angle relative to the x axis was identified. Circular statistics for comparison, were calculated using the Circular R package (Agostinelli – Lund 2022). Ellipses were identified from the 8-bit converted, threshold adjusted (42–182), and particle analysed QEMSCAN images. In R, wall angles were subtracted from the angles of the ellipses and the distribution of the angle differences were calculated using the Kernel Density Estimation (KDE) in the ggplot2 library (adjusted bandwidth 0.5) (Wickham 2016). To avoid the distributions falling at the edges, the data was replicated on both sides of 90 degrees. A measure of directionality was obtained by using the maximum density value for plagioclase, due to its size and abundance. Following these parameters, completely flat distribution would have a maximum frequency of 0.00185, with simulations of 232 random angles (the minimum plagioclase crystal number) giving maximum densities up to 0.00240, occurring at angles from -89° to 89°.

2.2.2 Scanning Electron Microscope

15 Specific grains were targeted for spot analysis using a JEOL 8530F Plus Electron Probe Microanalyser at the ANU-CAM to complement the identifications made by QEMSCAN. For every type of mineral identified by QEMSCAN, the chemical composition and stoichiometric ratios of ions from representative grains were obtained.

2.2.3. XRD

16 The XRD analyses were performed in the Research School of Earth Sciences of the ANU with a SIEMENS D501 Bragg-Brentano diffractometer equipped with a graphite monochromator and scintillation detector, using *CuKa* radiation. The scan range was 2 to 70° 2*q*, at a step width of 0.02°, and a scan speed of 1° per minute. To limit the impact of preferred orientation of the crystallites on XRD peak intensities each thin section was analysed twice, rotated by 90° in the diffraction plane, and the resulting XRD traces added. The results were interpreted using the SIEMENS software package Diffrac*plus* Eva 10 (2003). It has to be noted that performing XRD analysis on thin section, where minerals are embedded inside the clay can limit the ability of the instrument to identify minerals. In consequence, only a limited list of minerals was produced by XRD, compared to the QEMSCAN results. Still, XRD provided a baseline on which the complete list of minerals present could be compared with.

2.2.4. Petrography

17 Thin sections were observed at a range of magnifications from 20x to 200x under plane-polarised light (PPL) and cross-polarised light (XPL) using an Olympus CX31 optical polarising microscope with an Olympus LG-PS2 reflected light illuminator. Microscopic attributes relating to the nature of inclusions, clay matrix, internal structural

organisation and porosity pattern, and surface treatment and decoration were recorded for each sherd following standard ceramic petrographic descriptive systems and terminology (Quinn 2013). A rotatable stage and perpendicularly aligned polarising filters facilitated mineralogical identifications, with reference to petrographic atlases (Gribble – Hall 1985, Nesse 1991, MacKenzie – Adams 1994). Photomicrographs were imaged with an Olympus CS30 3MP or an Olympus BX53 and processed using Olympus Stream V1.9.1 imaging software.

3. RESULTS

3.1. Macroscopic features – Petrography

18 Most of the sherds bear parallel striations on either or both exterior and interior surfaces which indicates smoothing of the vessel surface prior to firing. Reddish-orange iron oxide-based paint had been applied on the surfaces of 72-2, 132-2 and 147-2. The decorations are limited to horizontal and possibly cross-hatched lines in reddish orange paint.

3.2. Mineral identification and abundance

3.2.1. Petrography

19 Dominant mineral inclusions are monomineralic (monocrystalline grains) in all samples. Plagioclase feldspar is consistently the dominant mineral inclusion (50–60%), followed by the amphibole group (10–20%). Other inclusions include quartz (5–10%) and minor clinopyroxene and orthopyroxene (<0.5–5%). The dominance of plagioclase feldspar and amphiboles in the coarse mineral fraction, as well as minor inputs of quartz and pyroxenes suggests that the ceramic raw material derived from of an igneous rock source intermediate to basic composition.

20 Polyminerallic rock fragments consisting of altered volcanic rock fragments of intermediate to basic composition (comprising plagioclase feldspar, amphibole and pyroxene phenocrysts) and possible tuff inclusions are present in all samples (5–15%). In addition to monominerallic quartz grains, quartz occurs as polycrystalline and microcrystalline fragments. Opaque iron oxide grains are observed in all samples (5–15%).

21 A high proportion of mineral grains were identified by QEMSCAN: over 98% of the minerals for seven samples (72-2, 76-1, 76-2, 116-2, 124-1, 132-1, 132-2), and 94% for the remaining three samples (50-2, 116-5, 147-2). The vast majority of minerals are well-defined grains and the majority of the quartz grains are monocrystalline. There are, however, numerous quartz-pixels that are isolated and dispersed across the clay matrix. These isolated quartz-pixels most likely represent sub-micron or silt-sized inclusions with high content in silicon and are therefore not included in further size or angle analysis given our minimum size threshold. Samples 124-1 and 132-1 had particularly high levels of these grains, while others (116-5 and 50-2) had few (Supplementary B).

22 The same range of minerals dominate every sample in comparable proportions (no statistical outlier), highlighting the homogeneity of the assemblage (Fig. 4, Fig. 5, Fig. 6). The relative proportion of plagioclase varies from 15.4% to 22.2%, with the exception of 147-2 (11.6%). Quartz is present at around 10-15% in the samples, except for 76-1 and 124-1 that have respectively low (6.8%) and high (16.7%) contents. Calcic amphiboles[1]

1 The ‘calcic amphibole’ category is composed of amphiboles for which the classification was ambiguous

represent roughly 3 to 6% of the mineralogical content of the samples, with only 124-1 showing a distinctively low content (2.2%). Iron oxides (hematite and magnetite[2]) and other minerals such as ulvöspinel, pyroxenes (hypersthene and augite) and orthoclase have minor abundances (<1% of the total). The mineralogical profile of the samples is completed by other marginal minerals, often just one or two grains per sample. The list includes minerals associated with igneous or metamorphic environments (ilmenite, rutile, zircon, diaspore, grossular-almandine, fayalite and kyanite), but some from sedimentary rocks (goethite) and less diagnostic chlorite and apatite. This mix of minerals is compatible with the local environment. The Dumoga sediment basin just east of Mansiri consists of alluvial sediments dominated by grey claystone, fine to coarse sandstone and gravels. It is boarded to the North and South by the Tapadaka formation, which consists of sandstones (also silicified), greywacke and shale. The Greywacke is fine to coarse grained composed of plagioclase, augite, quartz and a few hematite and magnetite minerals. To the West and East of the valley, Quaternary volcanics of the Pinogu formation are exposed. These are tuff, volcanic breccia and pyroxene andesites and dacite.

Fig. 4: Mineral compositions of the sherds as determined by QEMSCAN.

	50-2	72-2	76-1	76-2	116-2	116,5	124-1	132-1	132-2	147-2	50-2
Clay	54,1	65,9	68,9	69,1	60,1	60,4	54	64,1	68,2	67,4	54,1
Plagioclase	19,7	15,4	15,5	16,6	22,2	20	21,2	15,6	16	11,6	19,7
Quartz	9,1	10,9	6,8	9,2	10,9	9	16,7	13,4	9,5	11,4	9,1
Calcic amphibole	5,8	3,7	4	2,9	4,8	3,4	5,1	3,6	4,1	2,2	5,8
Iron oxides	3,8	1,9	2,5	0,4	0,7	0,3	0,1	0,9	0,6	1	3,8
Pyroxene	0,6	0,6	0,9	0,5	0,2	0,1	0,2	0,3	0,5	0,5	0,6
Unclassified	5,6	0,6	0,6	0,7	0,5	6,2	2,1	1,3	0,6	5,2	5,6

Fig. 5: Minerals identified by XRD.

50-2	quartz	plagioclase	amphibole		smectite	
72-2	quartz	plagioclase	amphibole		smectite	
76-1	quartz	anorthoclase	amphibole	orthopyroxene	smectite	tridymite
76-2	quartz	sanidine/albite	amphibole	orthopyroxene	smectite	tridymite
116-2	quartz	sanidine/albite	amphibole	orthopyroxene	smectite	
116-5	quartz	plagioclase	amphibole			
124-1	quartz	plagioclase	amphibole			tridymite
132-1	quartz	plagioclase	amphibole		smectite	tridymite
132-2	quartz	plagioclase	amphibole		smectite	tridymite
147-2	quartz	plagioclase				

even after analyses using high-resolution SEM-EDS. Compositional best fit is pargasite or some form of hornblende. However, calcic amphiboles in the ceramics appear to be solid solutions, which indicates that their compositions rests between these types. These calcic amphiboles differ from the pyroxene (augite) and orthopyroxene (enstatite/hypersthene) by their content in Na, as well as their lower content in Mg and Fe.

2 Preliminary observation of the QEMSCAN results showed that the magnetite analysis spots were systematically associated with hematite forming well-defined inclusions. As a result, it was decided to group these two minerals together under a common label (iron oxides).

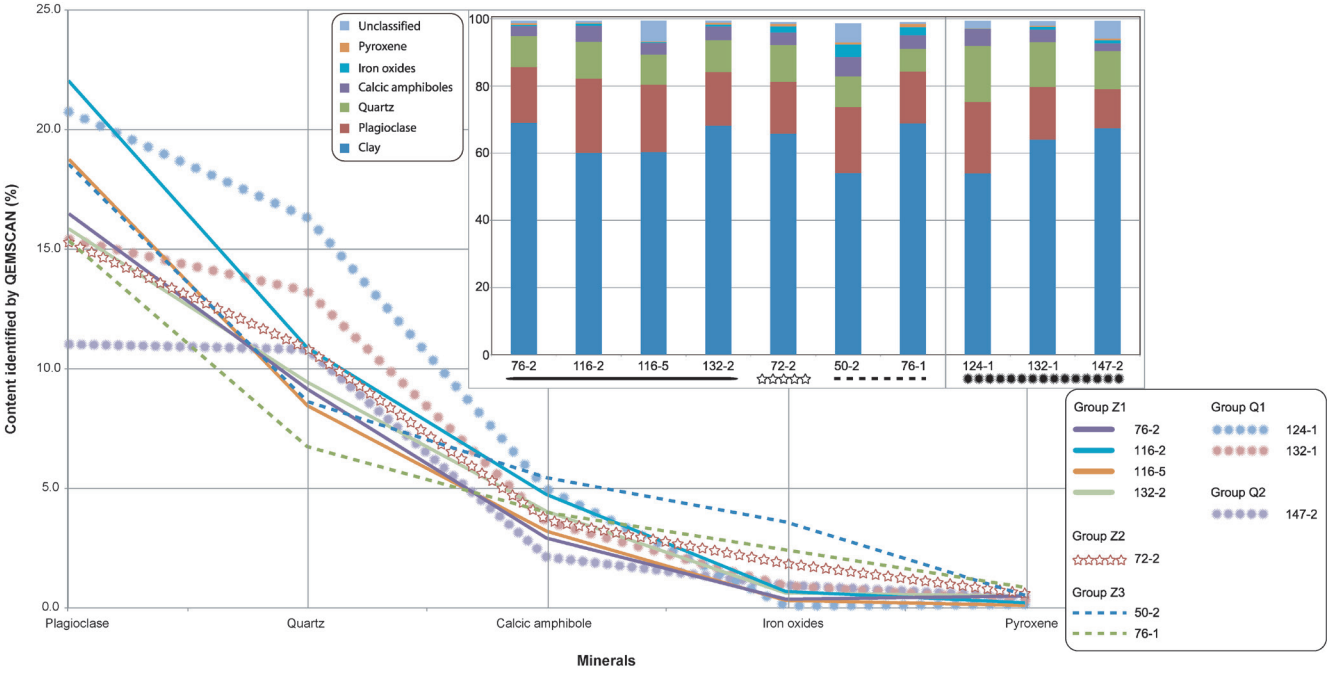

Fig. 6: Mineral compositions of the sherds as determined by QEMSCAN. The samples are grouped based on fabric variants (Z for dominant fabric dominated by plagioclase; Q for the fabrics with higher content in quartz).

3.3. Grain size and sorting

3.3.1. Petrography

23 Based on the petrographic analysis, the grains were estimated to be from fine sand-sized to gravel-sized. Modal size ranges varied from wide (300–400 µm for 50-2, 76-1, 116-2, 132-2) to narrow (350–370 µm for 72-2, 76-2, 116-5, 132-1, 147-2; 200 µm 124-1). Detailed results are in Supplementary C.

3.3.2. QEMSCAN

24 QEMSCAN data correlates well with the petrographic results. Frequency distribution charts of the grains larger than 4 phi show that the grain size distribution in our samples was primarily above 1 phi, with very few larger grains. These values reveal that the vast majority of the grains is included in the range between medium and very fine sand (Fig. 7). The code and relevant QEMSCAN images are available at http://doi.org/10.5281/zenodo.4285706.

25 Statistical analysis of grain size distribution (Fig. 8) reveals an absence of statistical outliers. Combined with the unimodal distribution of inclusions, this suggests that non-plastic inclusions were not manually added or, if temper was added, it had been manipulated and homogenised prior to inclusion, perhaps by levigation (Dal Sasso et al. 2014). No pattern of bimodality is evident from the frequency distribution charts, both for the entire range of minerals and for specific types. Only 147-2 shows a separated peak in its size distribution for grains of 2.25–2.50 phi but the trend is not pronounced enough to suggest bimodality.

26 The standard deviation of the phi values gives a measure of the sorting of the grains, i.e. the spread of the grain-size distribution (Boggs 2012: 57–59, Tucker 2001: 14). The samples have tightly distributed values within a range of 0.64 to 0.76; corresponding to moderately well sorted (0.50–0.71) and moderately sorted (0.71–1.00) deposits.

27 Skewness of the phi values is a measure of the symmetry of the distribution and the degree of peakedness is revealed by kurtosis. Every sample is significantly negatively skewed but again, the truncation caused by our minimal size threshold has an influence. Sample 116-5 has the lowest kurtosis and highest skewness, which means

Fig. 7: Particle size distributions for plagioclase, quartz, calcic amphibole and iron oxides (hematite and magnetite) in the sherd sections. Phi (-Log2 minimum Feret) was calculated from the QEMSCAN images. Percentages are of the total particles of the four minerals, measured, in the given range (0.5 to 3.75 Phi). The Kurtosis and skewness of the distributions are shown. Sherds are in order of increasing median Phi.

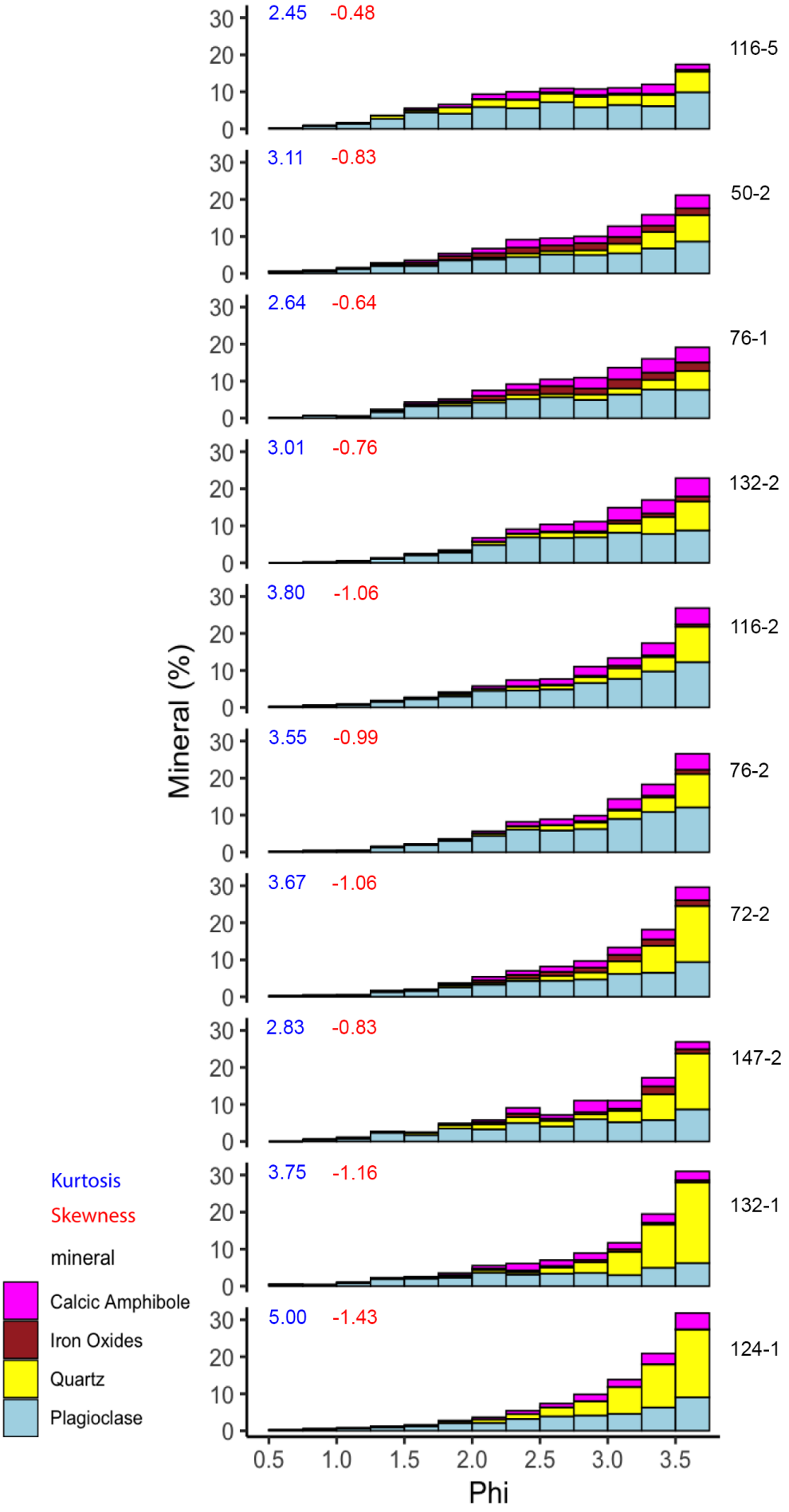

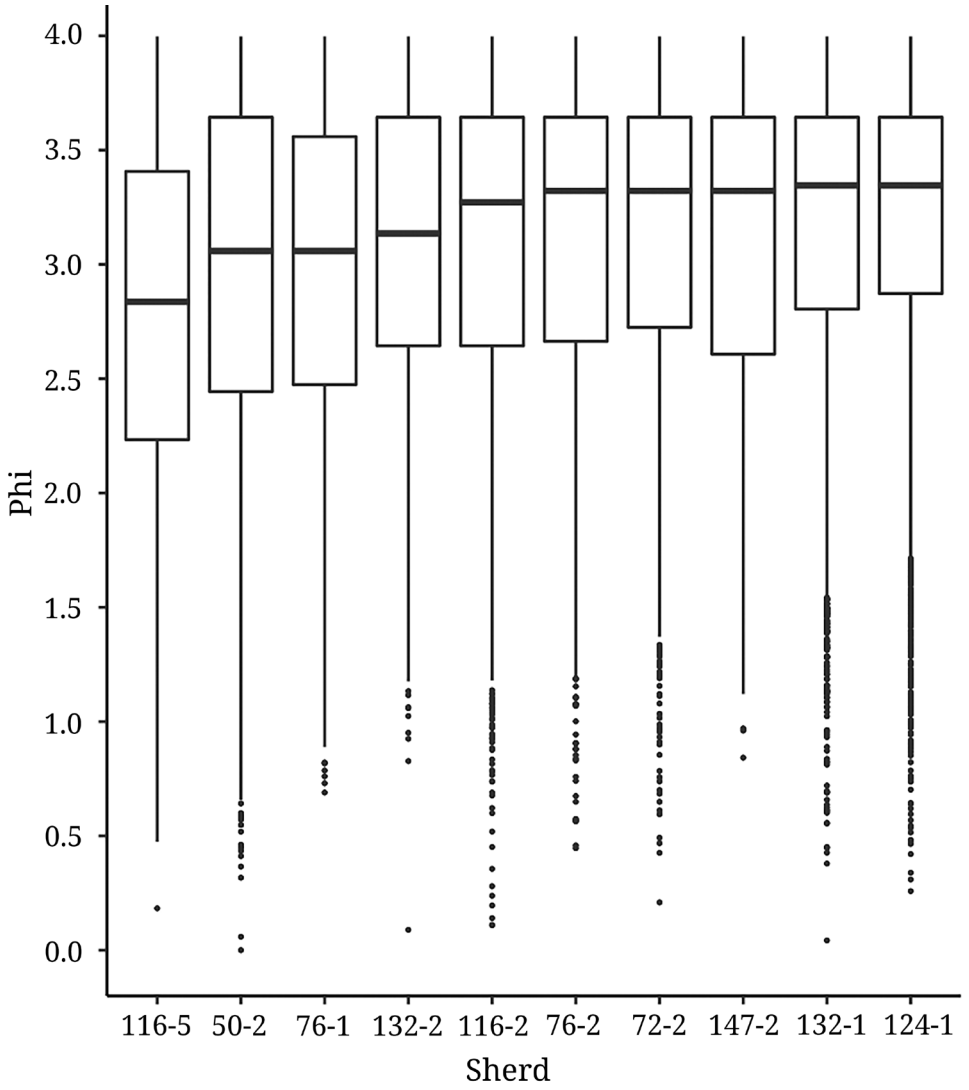

Fig. 8: Particle size distributions for combined plagioclase, quartz, calcic amphibole and iron oxides (hematite and magnetite) in the sherd sections. Phi (-Log2 minimum Feret) was calculated from the QEMSCAN images. Sherds are in order of increasing median Phi.

it has a wider range of modal sizes (2 and 3.75 phi) and more symmetrical distribution. It also has a higher proportion of larger grains (phi < 3) compared to the rest of the assemblage, particularly quartz grains. On the other hand, samples 72-2, 76-2, 116-2, 124-1 and 132-1 are better sorted, have sharper peaks, more prominent mode and consequently lower skewness and higher kurtosis.

3.4. Directionality

3.4.1. Petrography

28 Based on the petrographic analysis, the alignment of the grains was assessed to be generally sub-parallel in all ten samples. In addition, the petrographic observation of 132-1 and 124-1 revealed concentric alignments of inclusions representing relic coils, which is also evident on QEMSCAN maps (Fig. 9).

3.4.2. QEMSCAN

29 The grains were converted to ellipses and the difference in degrees between the angle of the (maximum) Feret diameter and the sherd wall was calculated to obtain their directionality (Fig. 10, Supplementary B). The distributions of the degree differences were examined to determine if any values occurred more frequently (Fig. 11). In many of the sherds, particularly those with higher levels of co-aligned minerals, plagioclase and calcic amphibole have a greater tendency to show co-alignment than quartz or

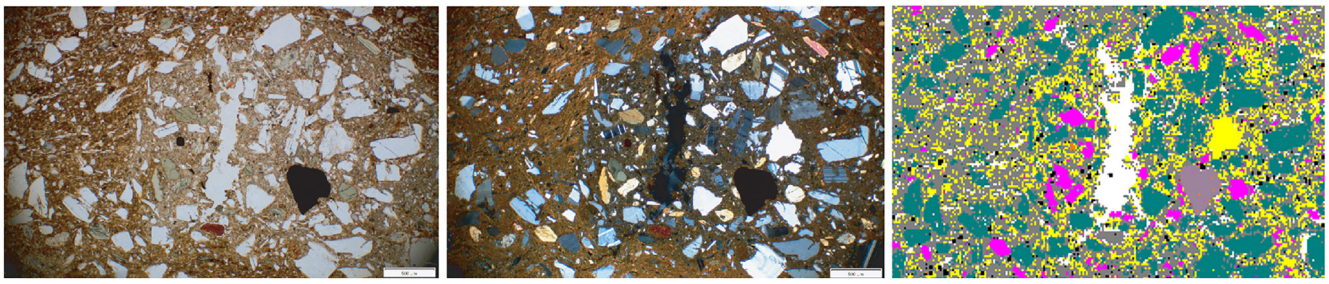

Fig. 9: Coil remnant from sherd 124-1, plane-polarised light (left), cross-polarised light (centre) and QEMSCAN image (right). QEMSCAN legend; grey: clay, blue: plagioclase, yellow: quartz, pink: calcic amphibole. Scale bar is 500 µm.

iron oxides. The alignment of plagioclase and calcic amphibole is probably related to manufacturing technique but the decreased alignment for quartz and iron oxide grains has probably more to do with their inherent attributes: quartz is often found as smaller inclusions (<0.2mm) for which it is more difficult to identify directionality. Iron oxides have fewer elongated shapes and circular shaped minerals are less likely to show directionality.

30 The similarity of the plagioclase curves for most samples is evident, with the maximal density occurring parallel to the surface of the sherds (angle difference less than 5° for both the mode and circular average) (Fig. 11). With the exception of one cut for 50-2 (50-2C), all plagioclase maximal densities were higher than the 0.00240 cut-off value suggested from random simulations. The most co-aligned/directional sherds are 76-2, 72-2, 116-2 and 50-2 with respective plagioclase maximal densities of 0.00429, 0.00397, 0.00386 and 0.00358.

31 The rim sherd 50-2 was cut in three locations to test whether the direction of the cut impacts the directionality index (Fig. 11 and Fig. 12). Direction A is a cross-section, perpendicular to the rim, Direction B is parallel to the rim and Direction C is at an angle of about 66° of the rim[3] (Fig. 3). 50-2B had the most co-aligned plagioclase grains (0.00358 maximal density), and these were aligned parallel to the sherd wall. Alignment at this orientation suggests coiling (although pinched or slab made could also be a possibility). The cross-section 50-2A had some degree of parallel alignment (0.00298 maximal density, at 4.8° to the wall angle) but it would be expected that pinching or slab building would give more strongly vertically aligned minerals (Berg 2009).

32 Samples 72-2 and 76-2 both had two sherds belonging to the same vessel scanned. It is difficult to interpret the alignment of their grains in relation to pottery manufacturing practices since they were all relatively small body sherds, which made the assessment of vessel orientation uncertain. However, they had strong indications of minerals aligned parallel to the wall (especially the cuts on both sherds A). If the sections were cross-sections this suggests they were slab-built, pinched or even moulded. Alternatively, if they were cut parallel to the rim, it is indicative of coiling (Berg 2009, Carr 1990). The alignment indicates that it is unlikely that drawing was used. All in all, paddle and anvil or beating as a secondary manufacturing technique with coiling as the primary forming technique is compatible with the results.

33 Samples such as 76-1, and 124-1 showed differences in the level of co-alignment in different areas of the section, with the thinner walls generally having higher maximal densities (Supplementary B) conceivably due to increased compression. Interestingly, the thinner, lower wall of the coil-made 124-1 had increased alignment with a maximal density of 0.00306. Thus, compression and smoothing of coils could result in a pattern similar to that in 50-2A.

3 This unorthodox cut was included to demonstrate the importance of the orientation of the cut. As expected, the angled section 50-2C showed little alignment, highlighting that poorly oriented sections have no interpretative value for forming techniques.

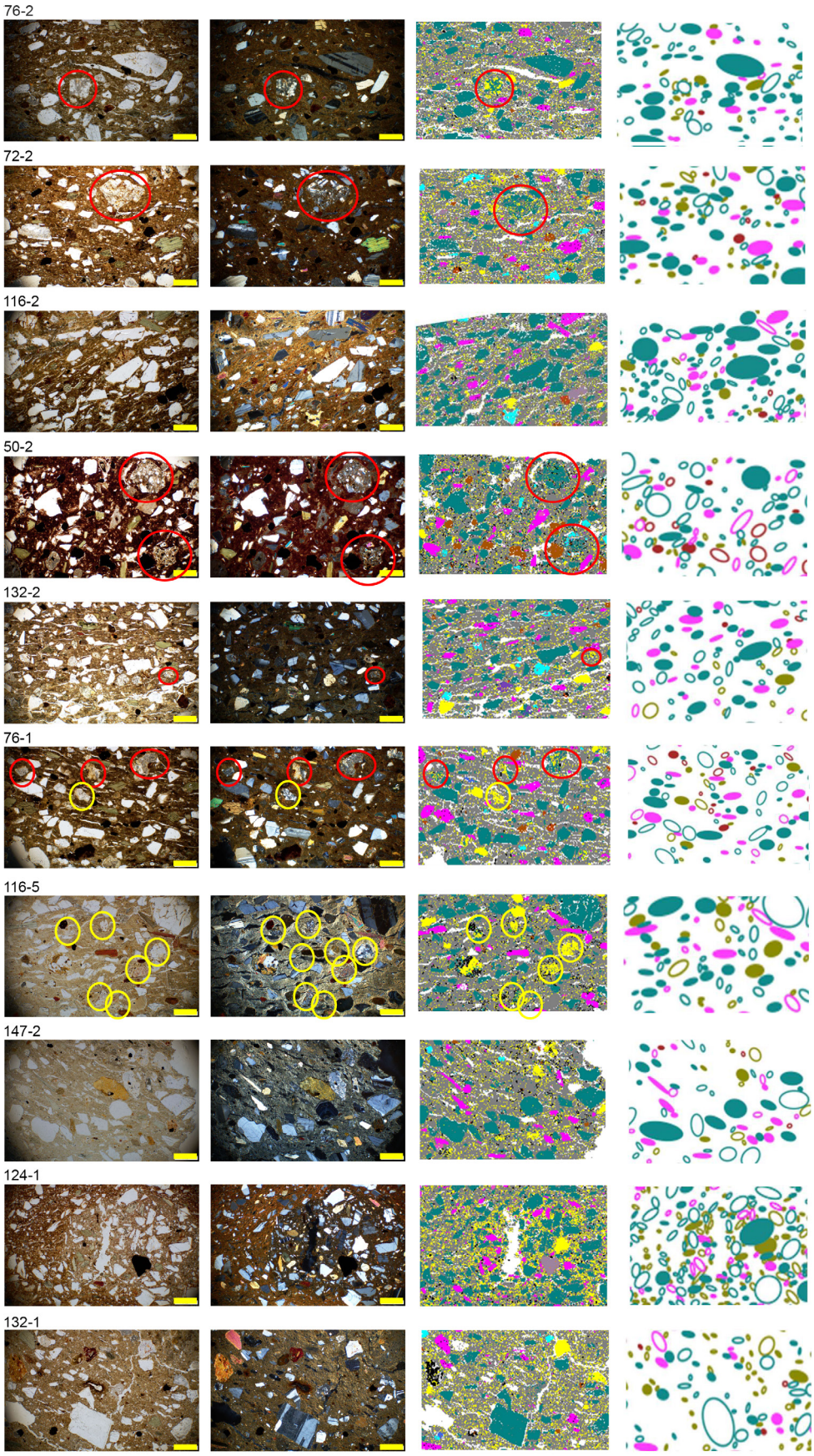

Fig. 10: Sample comparisons of PPL, XPL, QEMSCAN and representative ellipses for sherd sections. The ellipses were generated from automatic particle detection of QEMSCAN images to enable determination of particle angle. Typical rock fragments (red) and polycrystalline quartz (yellow) circled. QEMSCAN and ellipses colour scale; blue: plagioclase, yellow: quartz, pink: calcic amphibole, brown: iron oxides. Filled ellipses indicate minerals with an angle +/- 22.5° from the wall of the sherd. Scale bar is 500 µm.

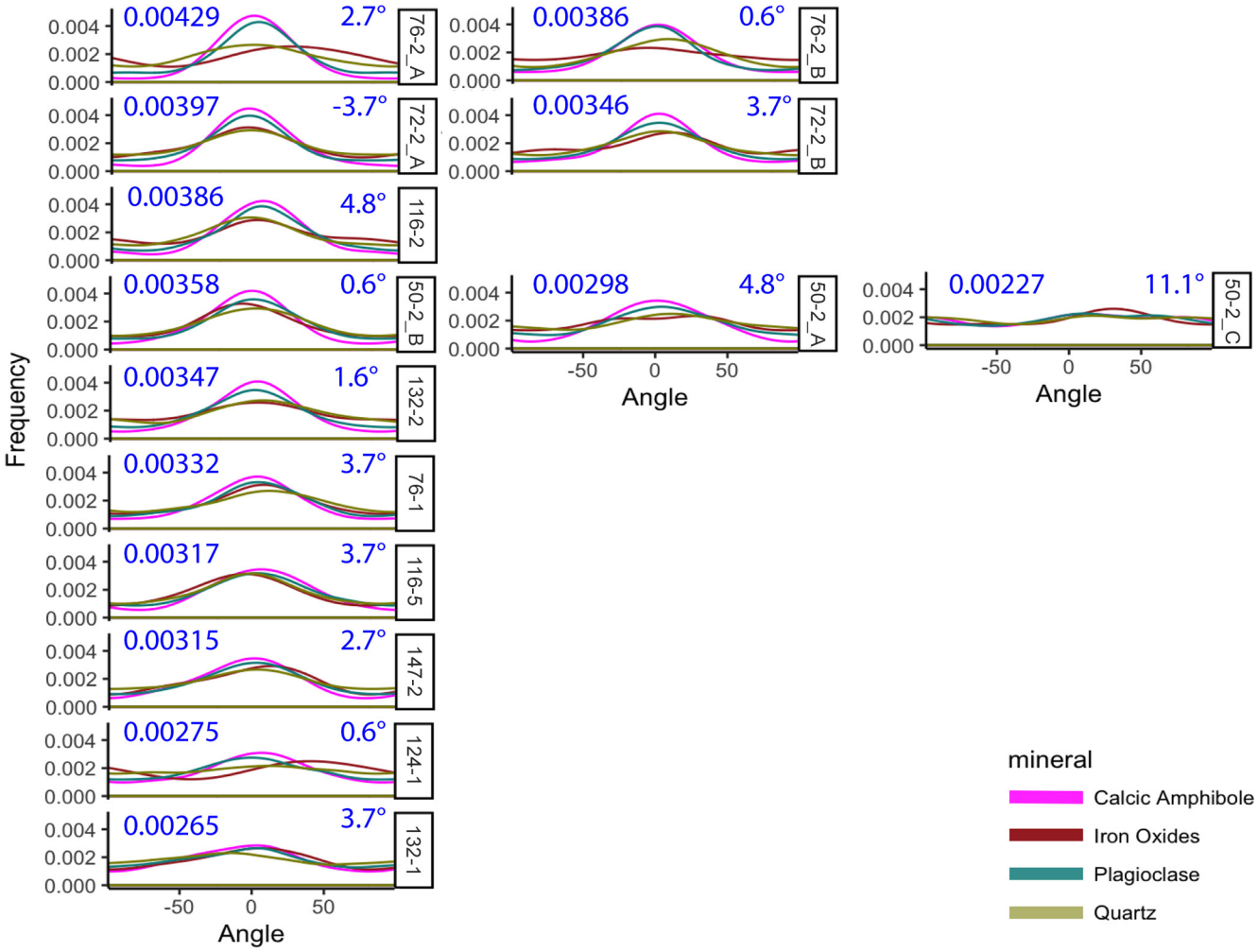

Fig. 11: The level of mineral co-alignment in the sherd sections and their degree of difference to the sherd wall. The frequency distributions of the angle differences of the minerals to the sherd wall were calculated. The maximum frequencies/densities for plagioclase, are indicated on the left, with the angle they occur at on the right. Several sherds had more than one section. Note simulations of random angles give maximum densities up to 0.00240, occurring at angles from -89° to 89°.

Fig. 12: The values for the circular average are included here for comparison with the mode in Figure 8. As expected, the results are comparable: the circular means are all within 5° of the sherd wall, with the exception of 50-2 C and generally the higher the distribution maximum frequency, the lower the standard deviation (or variance).

Sherd*	Circular Mean (°)	Circular Median (°)	Circular SD (°)	Circular Variance (°)
50-2 B	0,76	0,10	0,65	0,19
50-2 A	3,93	4,90	0,74	0,24
50-2 C	9,33	10,79	0,90	0,33
72-2 A	-3,28	-4,40	0,63	0,18
72-2 B	1,41	2,39	0,69	0,21
76-1	2,64	3,52	0,72	0,23
76-2 A	1,42	1,91	0,60	0,16
76-2 B	-2,01	-0,69	0,65	0,19
116-2	4,65	4,42	0,66	0,19
116-5	4,04	2,71	0,71	0,22
124-1	1,20	1,08	0,79	0,27
132-1	-2,88	-0,81	0,82	0,29
132-2	0,75	1,31	0,69	0,21
147-2	0,49	1,28	0,70	0,22

4. DISCUSSION

4.1. Clay source and manufacturing

34 Even though the collection is fairly homogeneous, subtle variations are observed between samples based on their content in quartz and iron oxides (Fig. 6). Samples 124-1 and 132-1 have the highest content in quartz, which is predominantly very fine grained. Samples 76-1 and 50-2 have distinctively high proportions of iron oxides that probably originate from similar albeit increasingly placered deposits compared to the other samples. Overall, the fabrics identified at Mansiri have similar proportions of the same mineral types (plagioclase, quartz, calcic amphibole and iron oxides) and comparable grain sorting. This suggests that every sample was manufactured from a similar raw material source, with the variations between samples reflecting different points on a continuum (i.e., slightly varied depositional or weathered environments within the general same area). The similarity of the grain-size distributions also supports a single source of clay (Quinn 2013: 103). Higher quartz/plagioclase ratio, and/or abundance of very fine quartz grains as observed in 147-2 can be assumed to originate from more weathered section of the source.

35 The general mineral composition is consistent with the clay being sourced locally, from the alluvial Dumoga sediment basin in which materials from the surrounding volcanic formations accumulates. Considering that valleys such as this one are depositional environments with high variability and gradation in grain size depending on proximity to alluvial landforms, the fine variability picked up by QEMSCAN represents normal intra-source variability.

36 Manually added tempers frequently have rounded grains and multi-modal grain size distributions, with the larger grains being the added material (Quinn 2013: 103, 161, 165). This fits well with the results of the grain-size analysis. First, the majority of the grains are sub-angular to sub-rounded and there is no sign of angularity compatible with deliberate crushing; second, the grain size distributions are well sorted to moderately sorted and unimodal; and third, quartz grains and fragments of shell or coral limestone are relatively rare. Consequently, the texture of these ceramic pastes suggest that non-plastic inclusions were naturally present in the clay which did not require manual addition of temper sand. Still, it is possible that the potters at Mansiri manipulated the raw materials. Sieving and levigation processes such as those utilising a mesh can result in a fine paste with a truncated, right-skewed, unimodal grain size distribution (Quinn 2013: 103, 154–156). This would be consistent with the negatively skewed grain size distributions of the Mansiri samples, with higher proportions of smaller grains (3–4 phi) compared to larger grains. Differing degrees of manipulation may also explain some of the variability among the samples, for example the clay for 116-5 containing larger inclusion, may have been subject to less processing.

37 In terms of manufacturing techniques, both paddle and anvil (72-2 and 132-2) and coiling (124-1, 132-1) were used at Mansiri. Data is consistent with coil-making being the primary forming technique with beating/paddle and anvil used as a secondary technique to smooth the surfaces, remove rilling and create the thinner walls. This contrasts with pottery from Kamassi and Minanga Sipakko, two Neolithic sites (3600–3000 BP) in the Karama Valley, West Sulawesi, where no evidence of coiling was identified and where the use of anvils, with slab and hand modelling was suggested (Anggraeni et al. 2014, Bulbeck – Nasruddin 2008; Simanjuntak et al. 2006). There is also evidence for the use of the paddle and anvil technique at other sites in the region such as Bukit Tengkorak, Leang Tuwo, Uattamdi, Matju Kuru 2 and Niah Caves (Chia 2003, Swete-Kelly 2017, Winter 2015).

38 Considering that several Northern Luzon sites (including Dimolit) show evidence of coiling with paddle and anvil finishing (Peterson 1974, Winter 2015), the ceramic technology at Mansiri, if indeed locally made, may have derived from the north rather than from within Sulawesi or to the East. This would be aligned with the suggestion made by Anggraeni et al. (Anggraeni et al. 2014) based on ceramic forms that ceramic assemblages in the region were related through shared heritage from the Philippines and Taiwan, rather than directly to each other.

4.2. Using QEMSCAN for pottery analysis

39 By the automated nature of its analysis, QEMSCAN increases the reliability and reproducibility of quantitative attributes such as size, sorting and orientation of the grains compared to petrographic analysis. QEMSCAN can also identify smaller particles more efficiently than petrography, as demonstrated by its ability to very fine quartz in some samples. For homogenous assemblages such as Mansiri, the systematic analysis of entire thin sections by QEMSCAN led to the identification of variants of fabrics. The quantitative data also contributes to a better understanding of technological aspects and we were able to determine both primary and secondary forming techniques. Lastly, the mineralogical maps produced by QEMSCAN have a limited colour range and clear distinctions between grains, which eases the segmentation of images. This is a significant advantage when using QEMSCAN data in combination with other analytical techniques such as microtomography for example.

40 As informative as QEMSCAN is, the identification of minerals in pottery samples is not a straightforward process and at risk of being inaccurate if the identifications made are not closely monitored. Additional analytical techniques, such as XRD or SEM-EDS, need to be used to verify them. This is particularly true for pottery for which several factors can affect its composition, which makes predicting the mineralogical content more precarious than other materials (e.g., using exotic raw materials different to local pedology, mixing of different raw materials by the potters, manipulation of the raw material (levigation, filtering), firing and post-depositional weathering). In our case, this situation was exemplified by the very similar chemistry between amphibole and pyroxene grains, for which SEM-EDS was essential to obtain accurate identifications by assessing the chemical composition (Na content is the main chemical difference between these minerals), stoichiometry and degree of hydration of the grains.

41 QEMSCAN is also afflicted by another limitation in regard to volcanic rock fragments, as illustrated notably by 50-2 and 72-2 (Fig. 10 and Supplementary B). In many cases, rock fragments were first identified as clusters of minerals. Manual curation can correct this on an individual basis, or perhaps programming an algorithm that would allow QEMSCAN to recognise clusters of minerals could be a valuable avenue for future research. However, currently, obtaining the proportion of rock fragments in a sample, is more easily achieved with petrographic analysis. On the other hand, QEMSCAN can help distinguish the type of rock through identification of the small constituent minerals, which can be hard to determine by petrography.

5. CONCLUSION

42 Automated mineralogical analysis achieved using QEMSCAN, along with the necessary contribution of petrography, XRD and SEM-EDS, successfully identified mineralogical content and manufacturing techniques for pottery from Mansiri. Based on the quantitative data extracted from the samples, it was possible to establish that

the raw materials correspond with the naturally available clay deposits near the site and that temper was probably not manually added. It was also demonstrated that two manufacturing techniques were used sequentially, with coiling as the primary forming technique and beating/paddle and anvil used as a secondary technique to smooth the surfaces.

43 However, it is clear that QEMSCAN has to be used in specific circumstances and/or with specific goals in mind (homogenous collection, large number of samples, established database already established for region/type of material, visualisation, etc.) to be most effective. It is particularly appropriate for samples with known or expected composition, or perhaps for refined investigation of homogeneous assemblages. QEMSCAN's efficiency relies entirely on the quality of the reference database used to identify mineral. Establishing a database for a specific region and/or for a specific type of material is an iterative process in which SEM-EDS, and XRD are necessary steps. As such, QEMSCAN is not the most straightforward exploratory approach to investigate new archaeological collections for which the range of minerals is relatively unpredictable. The time and efforts put into setting up a reliable reference collection will pay off mostly if streamlined high-throughput quantitative analysis is the objective. We think QEMSCAN can reach its full potential for pottery as part of an established protocol of research aiming to develop reference databases for various regions and/or types of material.

44 The study presented here represents a step forward in exploring how the technological study of pottery fabrics can contribute to further our understanding of Sulawesi's past. While previous studies in the area have focussed on decorative and morphological aspects of pottery assemblages, this study demonstrates that technological analysis provides additional elements in improving our understanding of past occupations on the island.

ACKNOWLEDGEMENTS

45 Constructive discussions about QEMSCAN with Prof. David Killick from the University of Arizona and Dr Michael Anenburg from the Research School of Earth Sciences at the ANU helped to improve previous drafts of the paper. The research was supported through an Australian Research Council Discovery Early Career Research Award to Christian Reepmeyer (DE130100046).

Supplementary A

Geological background Mansiri

46 The North Sulawesi arm (defined as part of the island North of 1° S) is a section of a Neogene island arc stretching from the Gulf of Tomini to include the islands of Sangihe in the Northeast. It is located at the intersection of three tectonic plates, the Southeast Asia, Pacific and Indian-Australian plate, which results in a very active volcanic region (Hall 2002). Sulawesi has undergone multiple subduction events from the Early Cretaceous, the mid-Oligocene and the lower Miocene (Kavalieris et al. 1992). These events resulted in a complex stratigraphy of blueschist and ophiolite complexes, followed regionally by basalt and andesitic volcanics. The Northern Arm of Sulawesi was primarily associated with the latest event, occurring in the Early Miocene (22-16 Ma) and Pliocene/Quaternary (later than 9 Ma). The lower Miocene formations primarily consist of calc-alkaline volcanics (pyroxene andesites or basalts, andesitic greywacke and minor uplifted limestone). Quaternary magmatism is not well understood on the North Sulawesi arm, but most likely includes both felsic and mafic rock types. Rhyolites, dacites, andesites and basalts occur, and are sometimes intruded by small quartz diorite dykes. The Lake Moat caldera, most closely located to the Dumoga valley is characterised by dacitic ignimbrites and hornblende andesite domes.

47 The formations associated with the Dumoga valley have been described in the geological map of Kotamobagu, by Apandi and Bachri (Apandi – Bachri 1997). The Dumoga sediment basin consist of alluvial sediments dominated by grey claystone, fine to coarse sandstone and gravels, and is weakly consolidated. It is boarded to the North and South by the Tapadaka formation, which consists of sandstones (also silicified), greywacke and shale. The Greywacke is fine to coarse grained composed of plagioclase, augite, quartz and a few hematite and magnetite minerals. Sandstones, mostly green in colour, contain feldspars, and few pyrite and chalcopyrite minerals. To the West and East of the valley quaternary volcanics of the Pinogu formation are exposed. These are tuff, volcanic breccia and pyroxene andesites and dacite. The felsic components of the lava formation contain both biotite and hornblende phenocrysts. Tuffs are commonly pumiceous, fine to coarse grained and light yellow. Volcanics as well as tuffs are weakly to moderately consolidated. Finally, the catchment of the Dumoga valley also contains early to late Miocene rocks of the Bilungala formation which are primarily andesite, dacite and rhyolite lavas, breccias and tuffs. Breccias and tuffs are weakly consolidated. The dacite lava is yellow to brown in colour and contains pyrite mineralisation and dioritic intrusive rocks.

Thin section preparation

48 Each sample was impregnated with epoxy resin under vacuum and were mounted to glass slides and ground to a standard thickness of 30 µm for petrographic examination. QEM-EDS and XRD were performed directly on the thin sections due to the limited size of the pottery sherds. This provided an added advantage of producing directly comparable results between the different methods. Prior to QEM-EDS analyses, thin sections were polished using a <1 um diamond-based polishing medium and submersed in an ultrasonic bath with deionised water for 30 seconds to remove any leftover residues from polishing. The samples were then coated with a 20 nm layer of carbon using a Dynavac CS300 coating unit in order to prevent buildup of static charge during exposure to the electron beam.

Supplementary B

49 For each sample, photos of cross sections (left) are juxtaposed with QEMSCAN maps (centre) and sections where minerals were converted to ellipses in order to estimate the axis angle for each mineral grain (right). The scale displayed is accurate for cross sections. Representative ellipses for mineral grains were generated from automatic particle detection of QEMSCAN images to enable determination of particle angle. Filled ellipses indicate minerals with an angle +/- 22.5° from the direction of the wall of the sherd (indicated by the red line). The maximum frequencies/densities for plagioclase, are indicated for each section, with the angle they occur at. The numbered rectangles correspond to areas for which photomicrographs in plane- and cross-polarised light are available in the following figure. The colours corresponding to mineral grains are shown in Fig. 13.

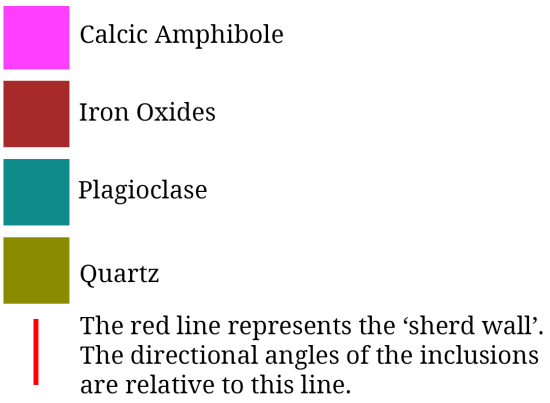

Fig. 13: Legend for Fig. 14–33.

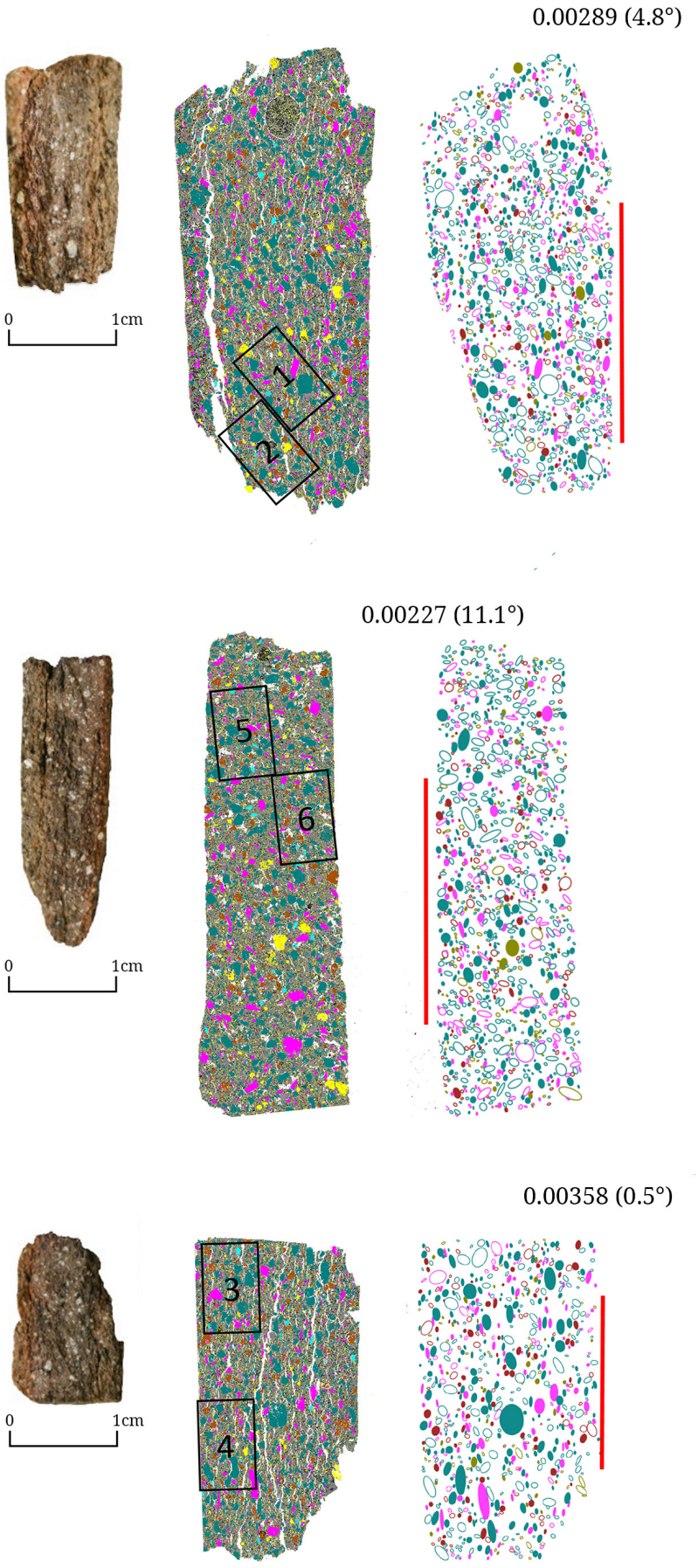

Fig. 14: Cross section, QEMSCAN map and ellipses for sample 50-2 A (top), C (middle) and B (bottom).

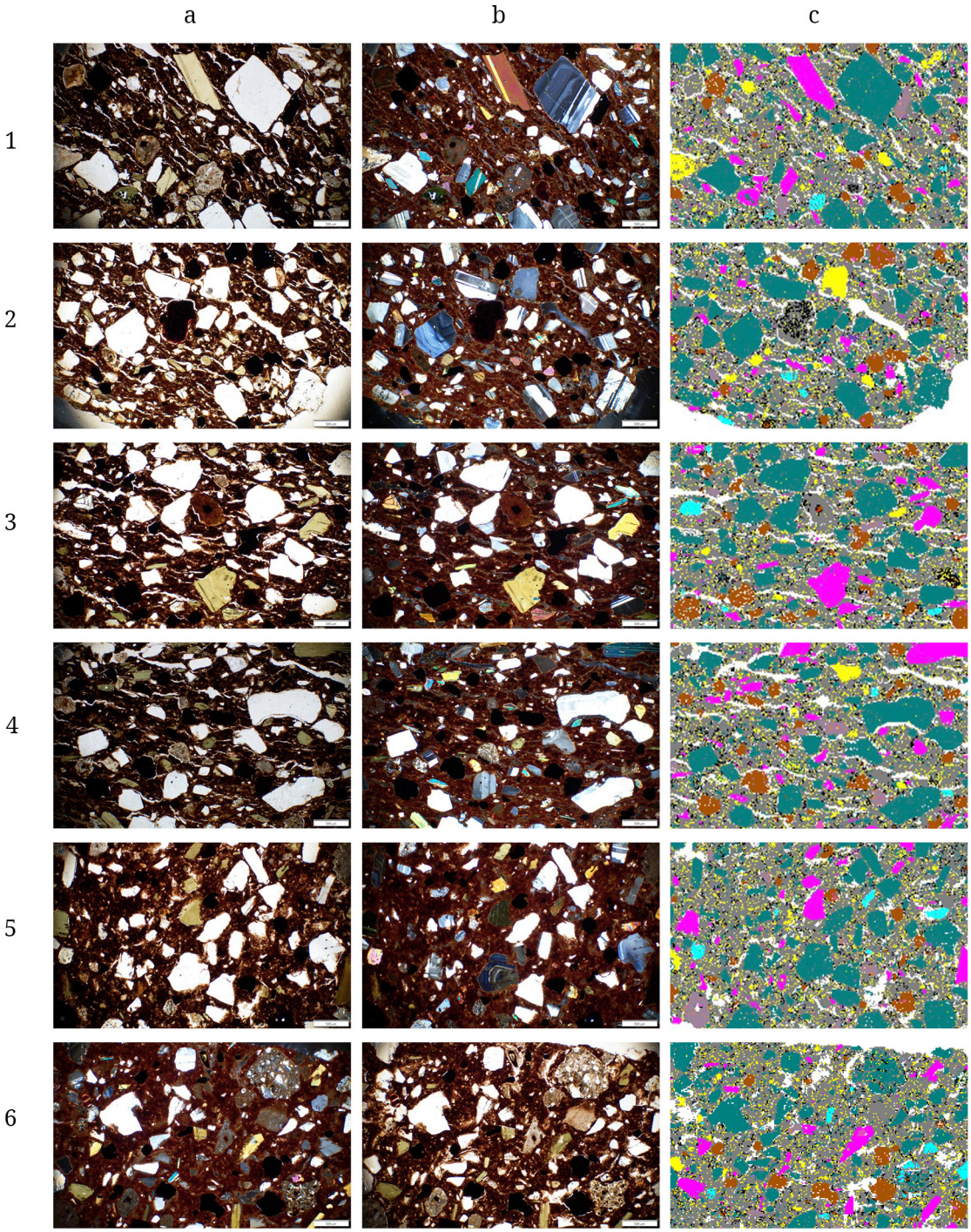

Fig. 15: Sample 50-2: Photomicrographs in plane- (left) and cross-polarised (centre) light, with the corresponding section of the QEMSCAN map on the right. The numbers correspond to the rectangles in Fig. 14.

Sample 72-2 Fig. 16, Fig. 17

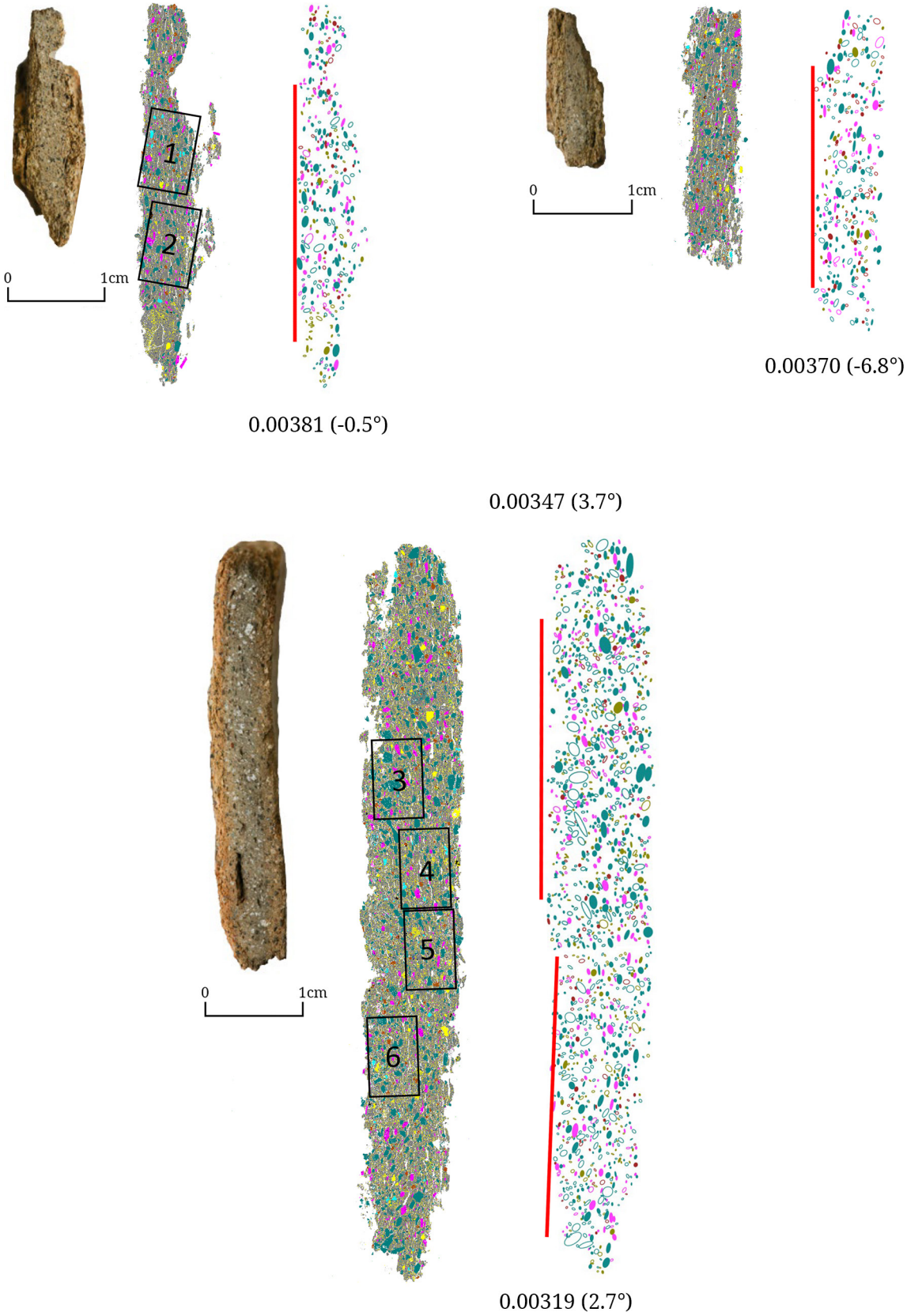

Fig. 16: Cross section, QEMSCAN map and ellipses for sample 72-2 A (top) and B (bottom).

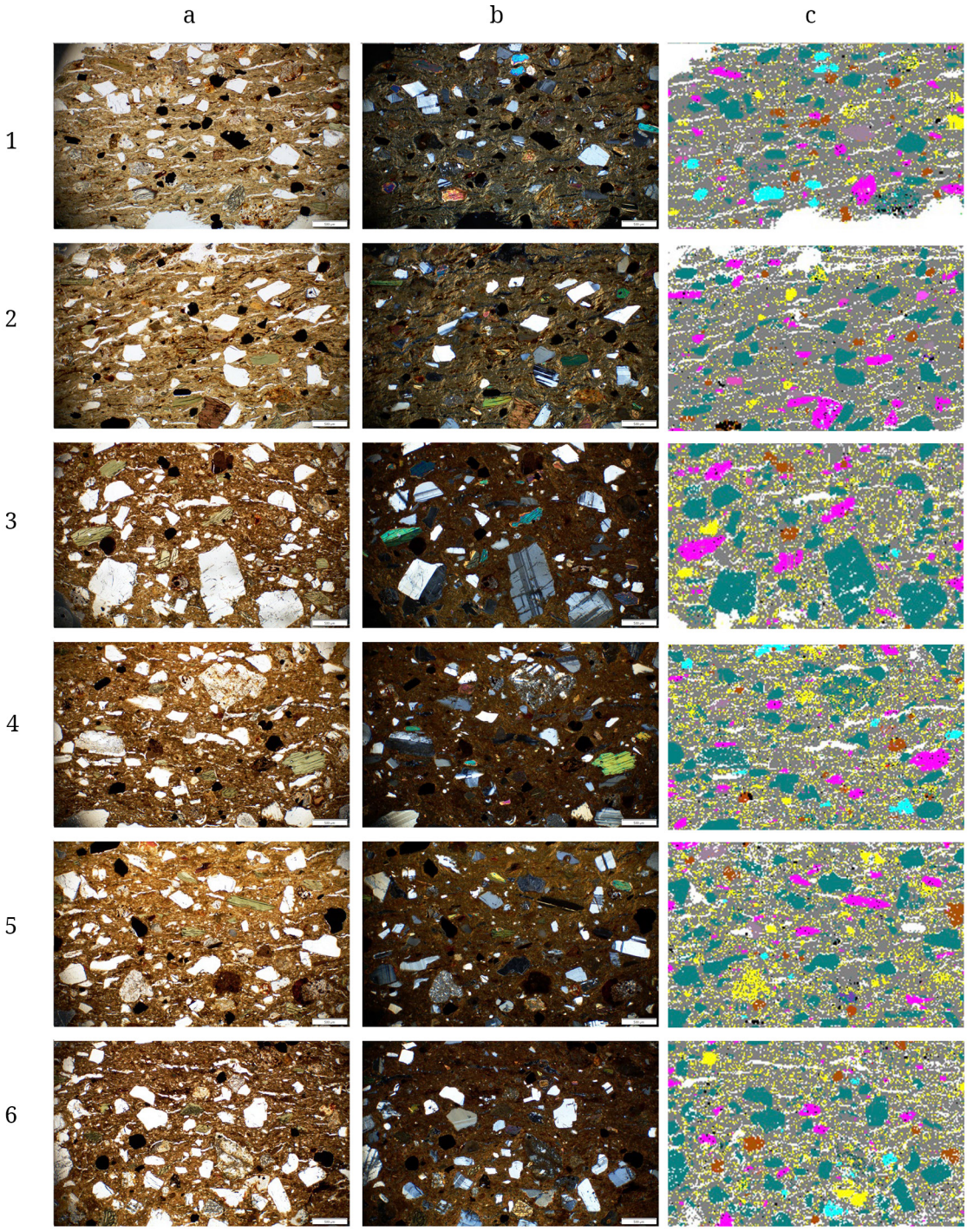

Fig. 17: Sample 72-2: Photomicrographs in plane- (left) and cross-polarised (centre) light, with the corresponding section of the QEMSCAN map on the right. The numbers correspond to the rectangles in Fig. 16.

Sample 76-1 Fig. 18, Fig. 19

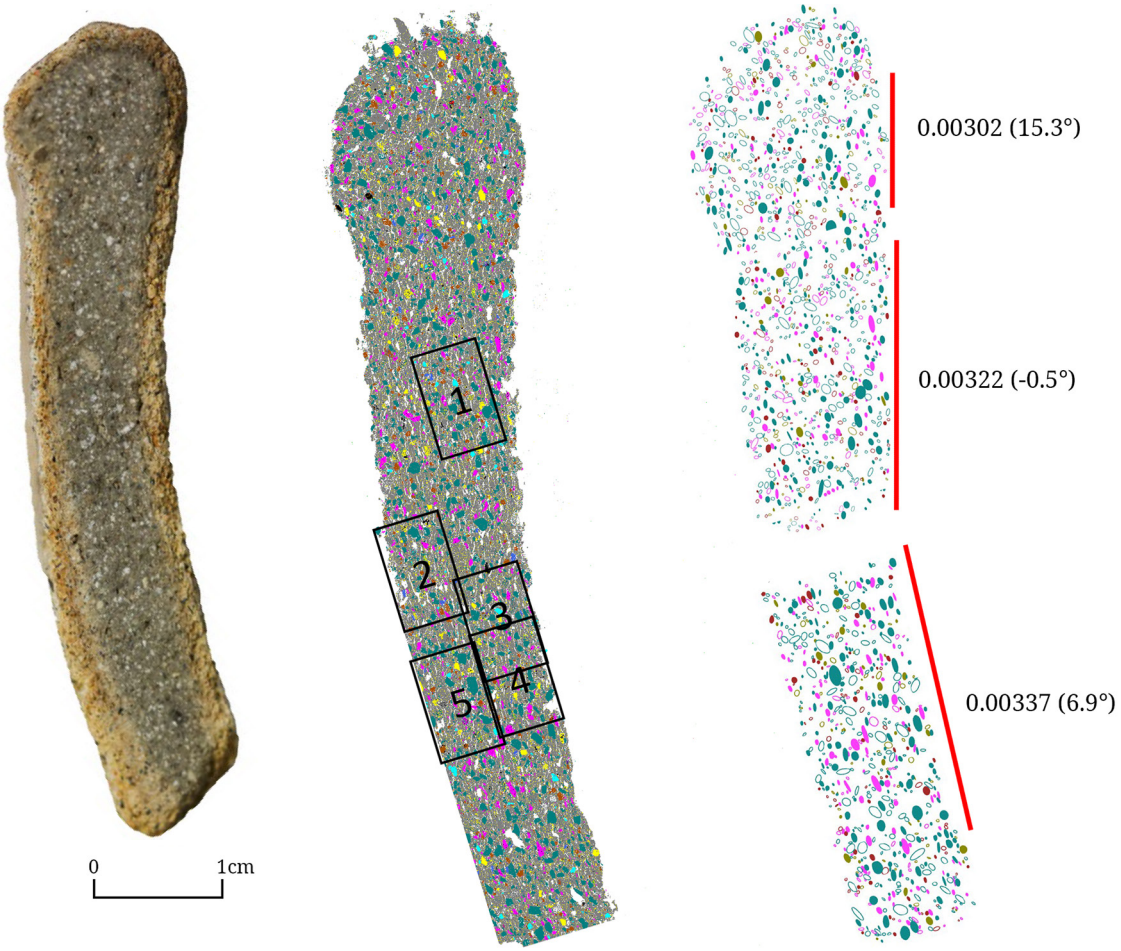

Fig. 18: Cross section, QEMSCAN map and ellipses for sample 76-1.

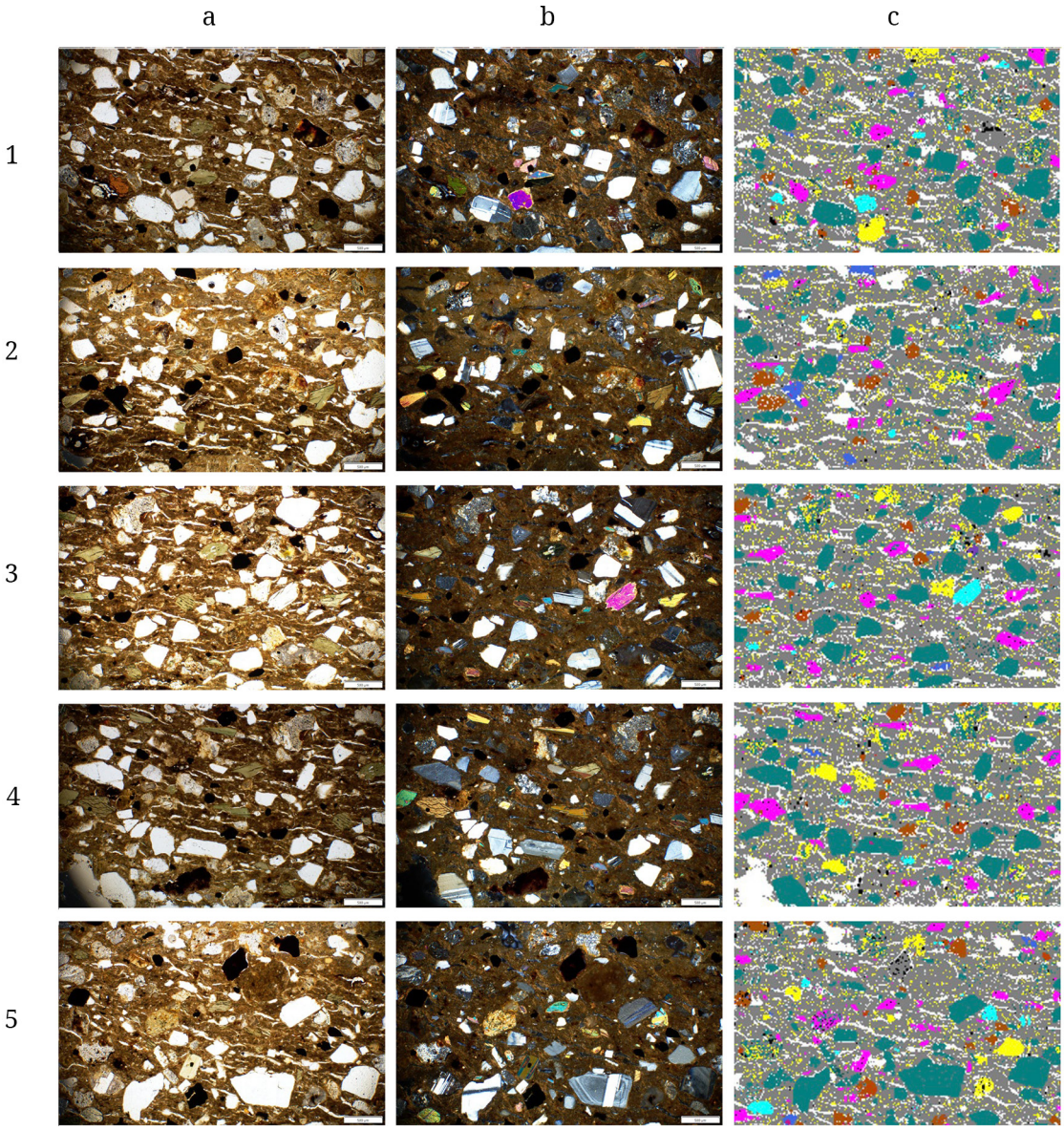

Fig. 19: Sample 76-1: Photomicrographs in plane- (left) and cross-polarised (centre) light, with the corresponding section of the QEMSCAN map on the right. The numbers correspond to the rectangles in Fig. 18.

Sample 76-2 Fig. 20, Fig. 21

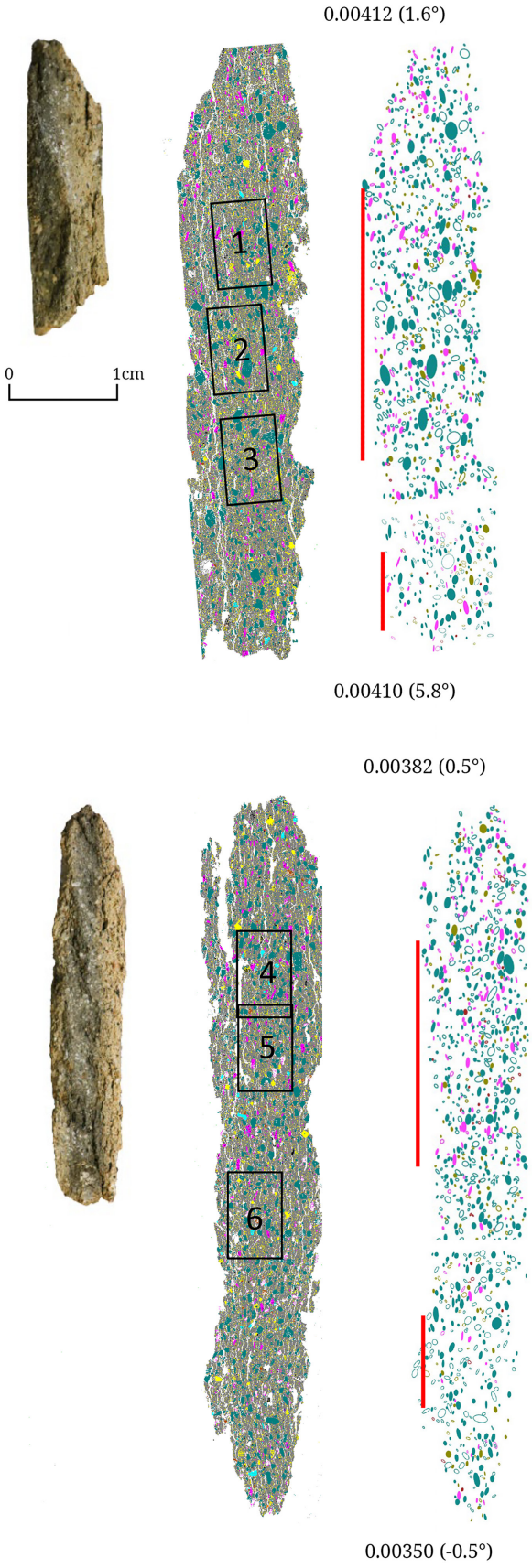

Fig. 20: Cross section, QEMSCAN map and ellipses for sample 76-2 A (top) and B (bottom).

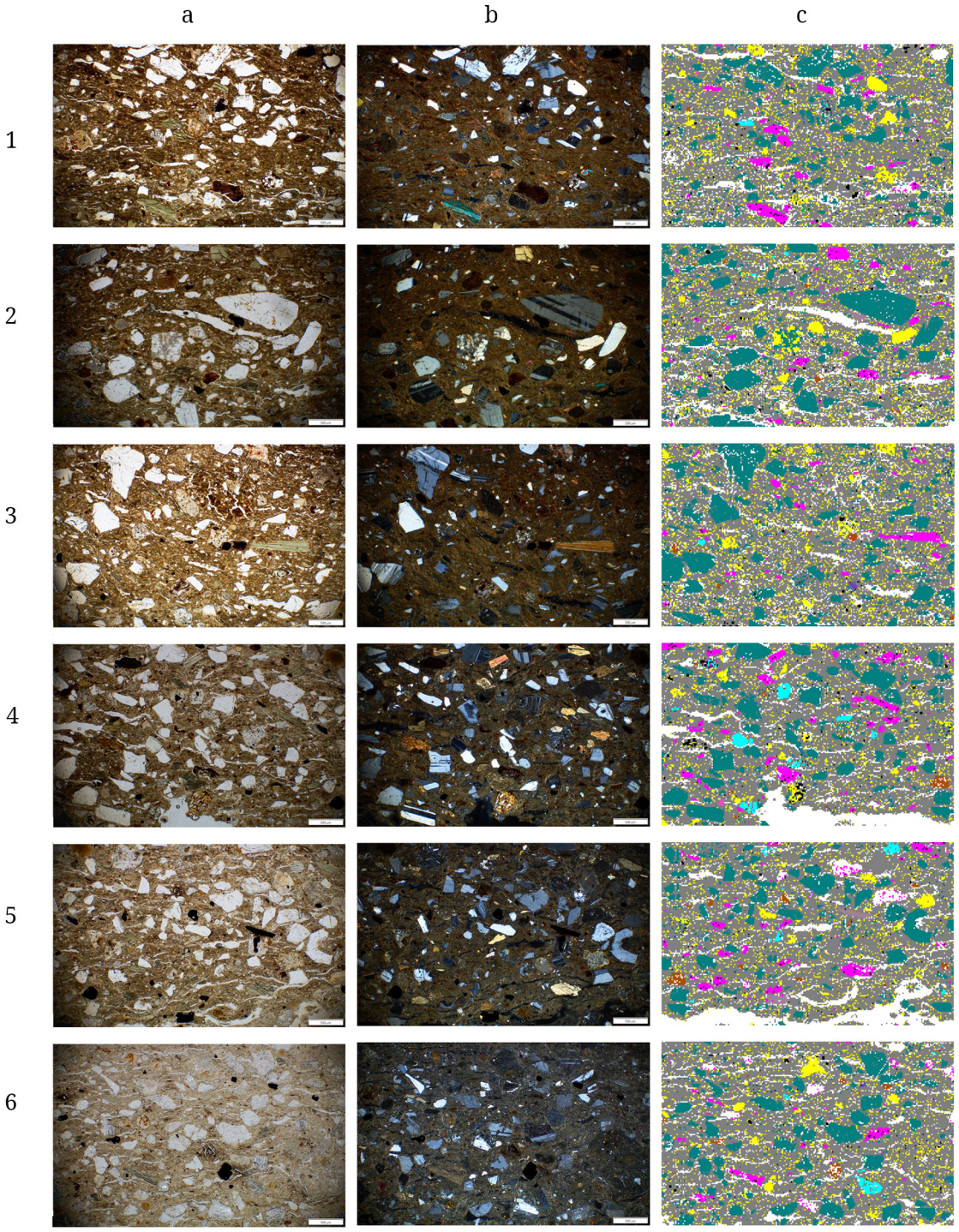

Fig. 21: Sample 76-2: Photomicrographs in plane- (left) and cross-polarised (centre) light, with the corresponding section of the QEMSCAN map on the right. The numbers correspond to the rectangles in Fig. 20.

Sample 116-2 Fig. 22, Fig. 23

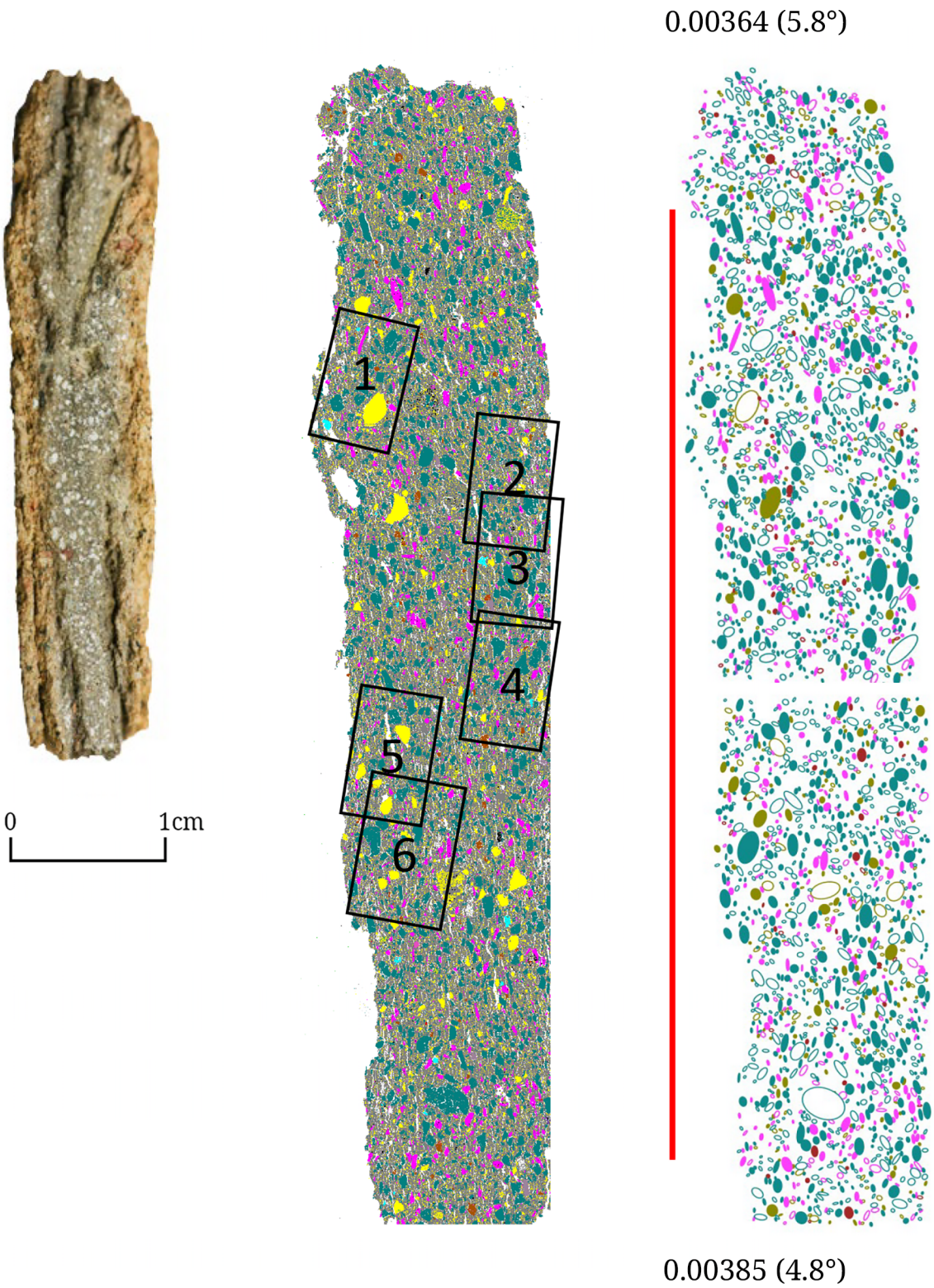

Fig. 22: Cross section, QEMSCAN map and ellipses for sample 116-2.

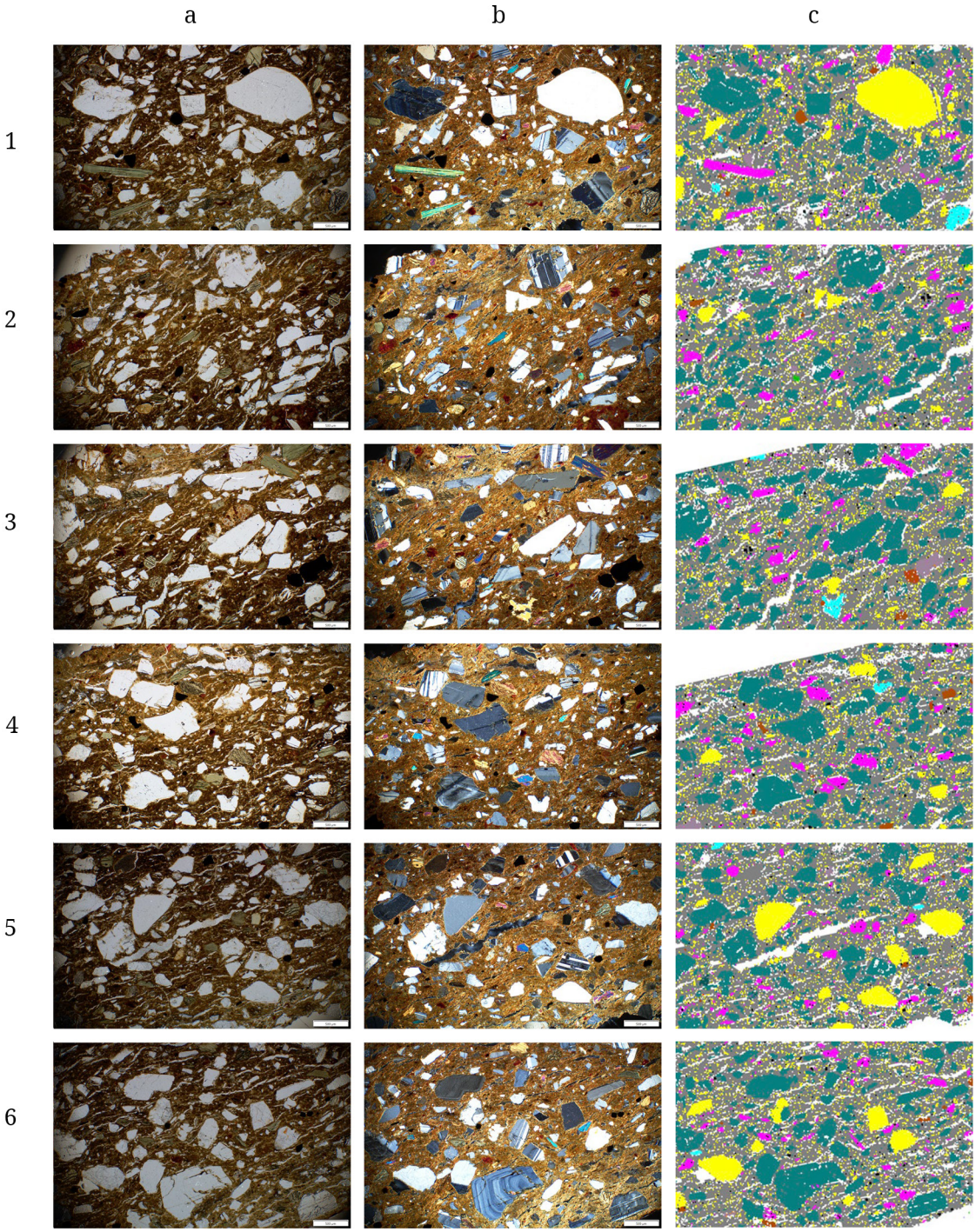

Fig. 23: Sample 116-2: Photomicrographs in plane- (left) and cross-polarised (centre) light, with the corresponding section of the QEMSCAN map on the right. The numbers correspond to the rectangles in Fig. 22.

Sample 116-5 Fig. 24, Fig. 25

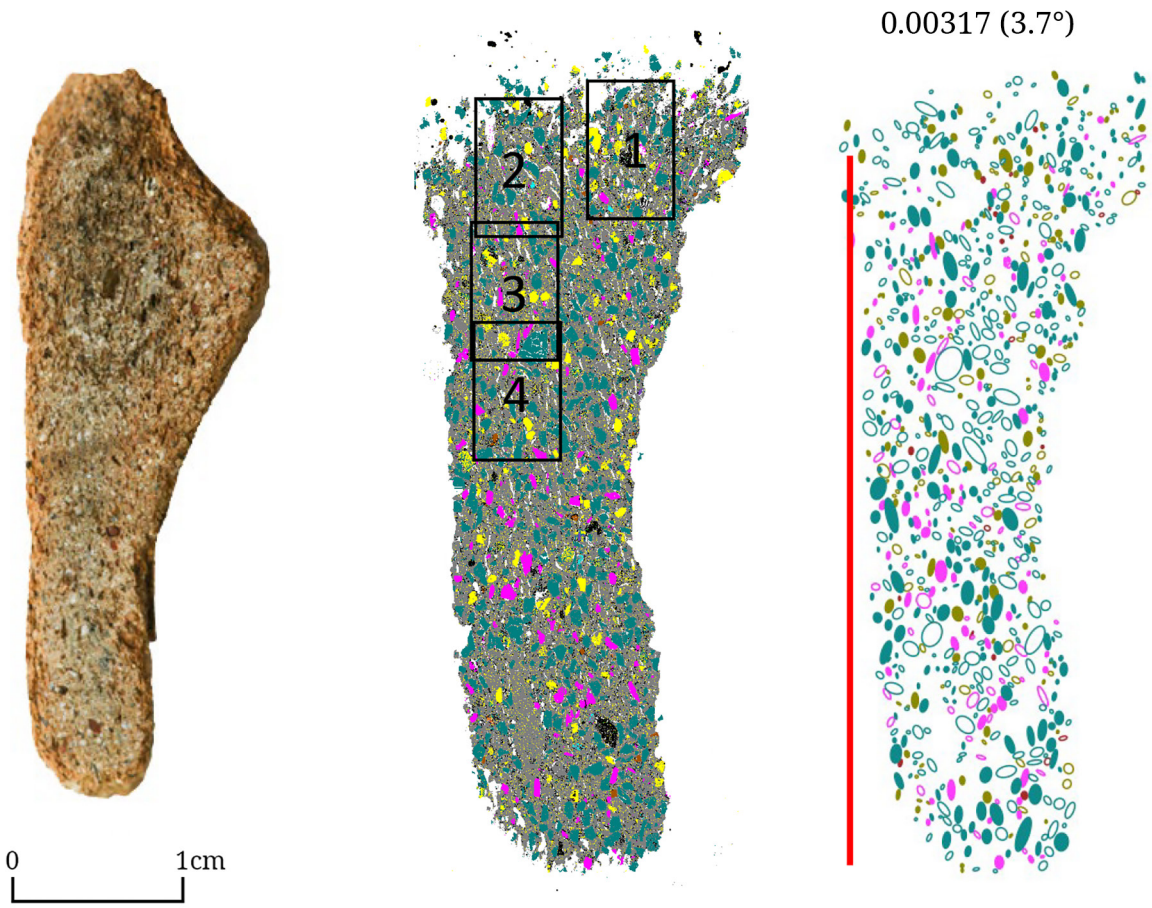

Fig. 24: Cross section, QEMSCAN map and ellipses for sample 116-5.

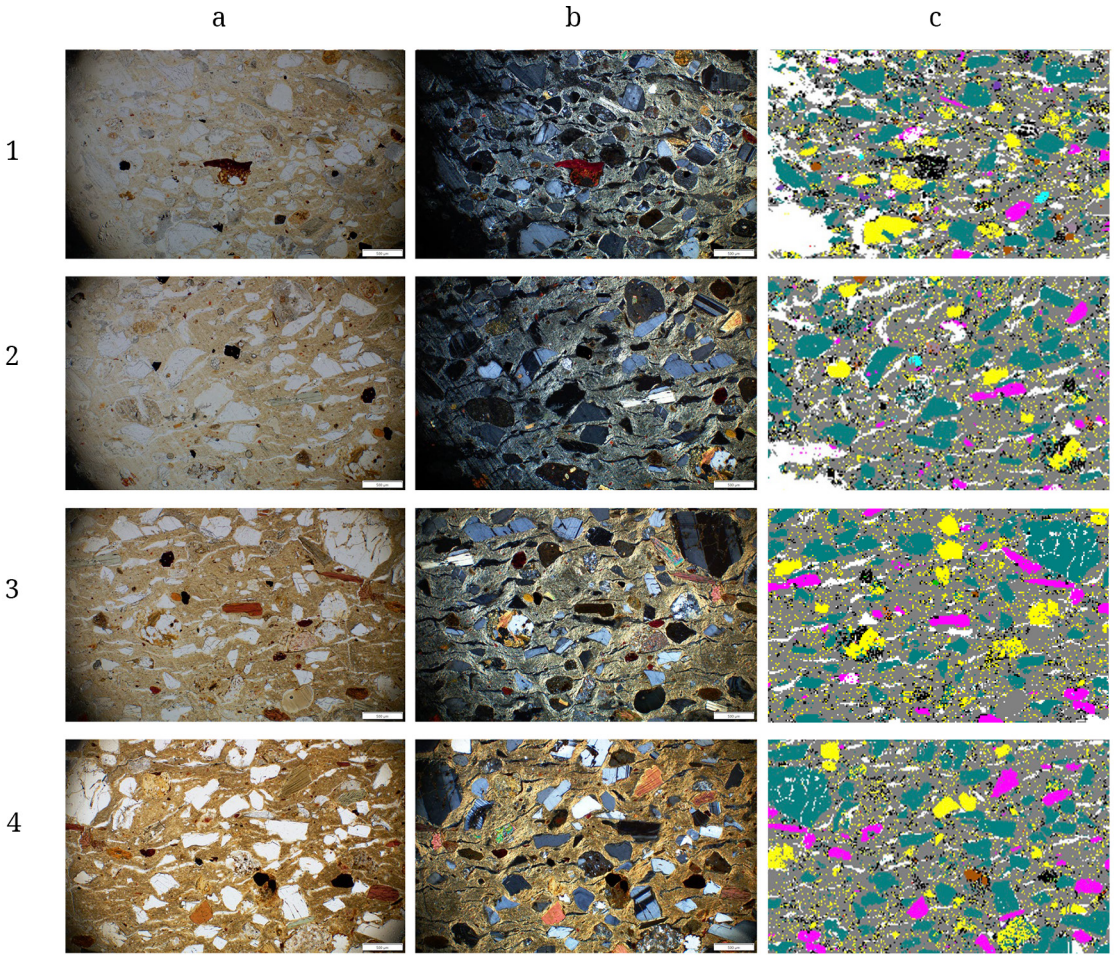

Fig. 25: Sample 116-5: Photomicrographs in plane- (left) and cross-polarised (centre) light, with the corresponding section of the QEMSCAN map on the right. The numbers correspond to the rectangles in Fig. 24.

Sample 124-1 Fig. 26, Fig. 27

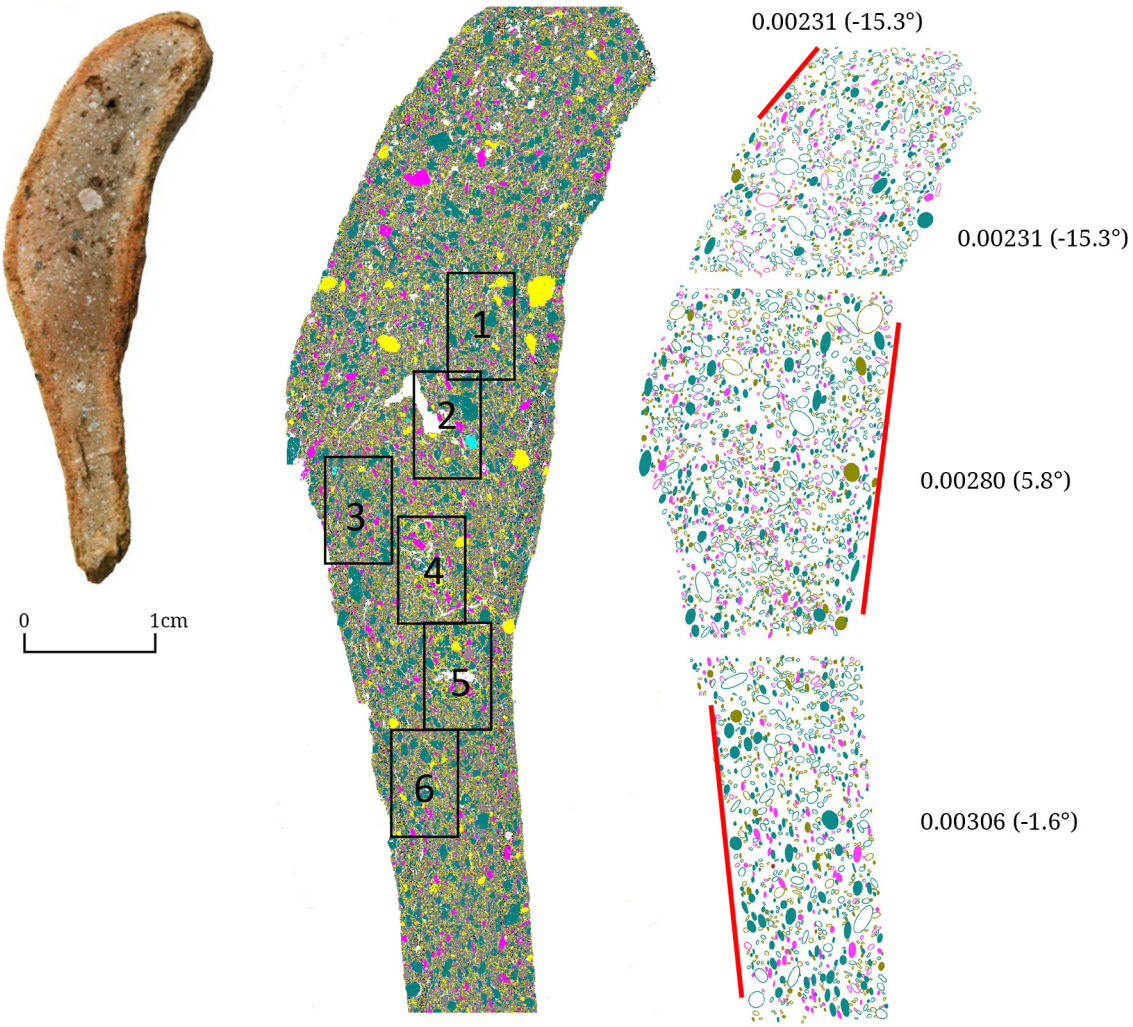

Fig. 26: Cross section, QEMSCAN map and ellipses for sample 124-1.

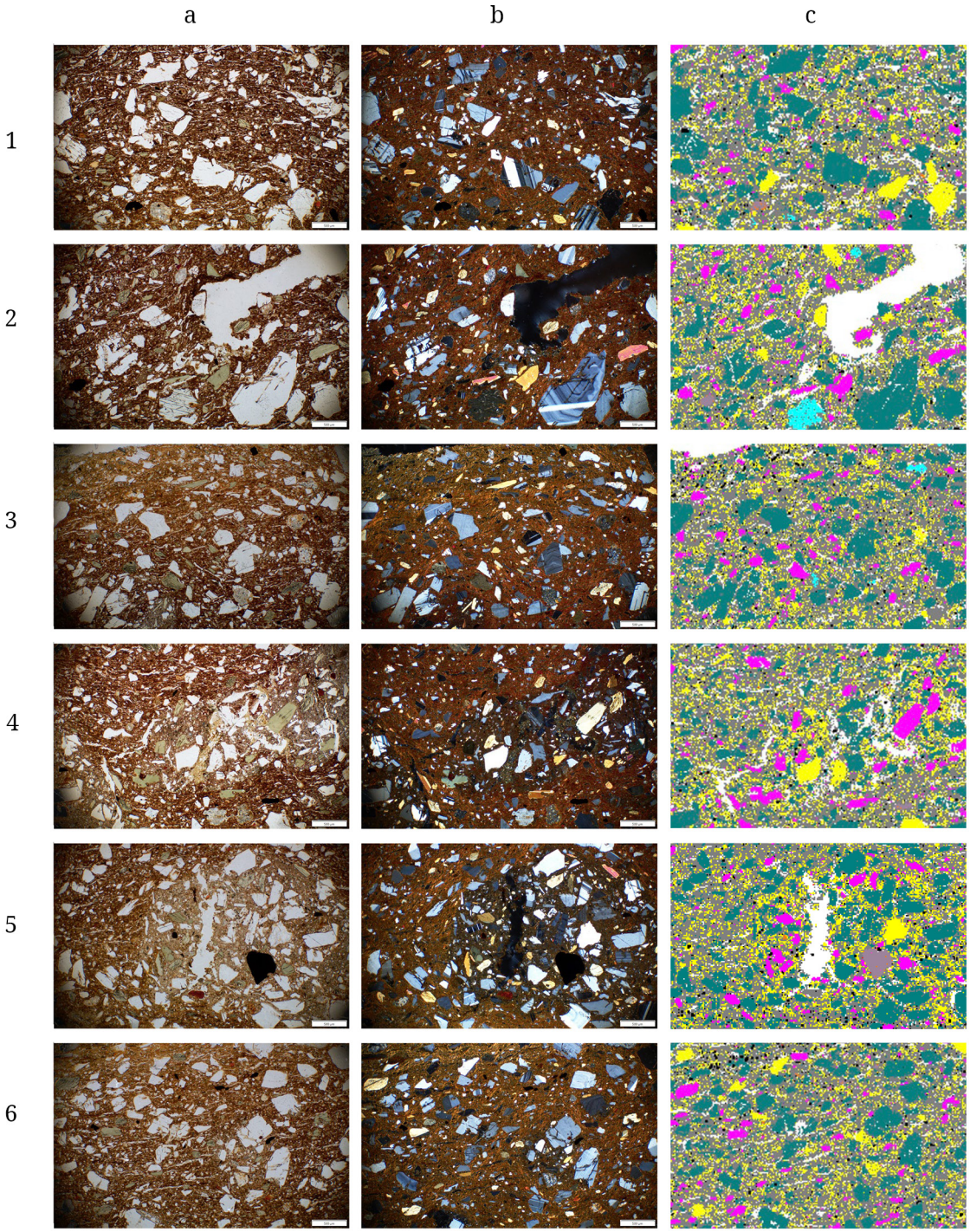

Fig. 27: Sample 124-1: Photomicrographs in plane- (left) and cross-polarised (centre) light, with the corresponding section of the QEMSCAN map on the right. The numbers correspond to the rectangles in Fig. 26.

Sample 132-1 Fig. 28, Fig. 29

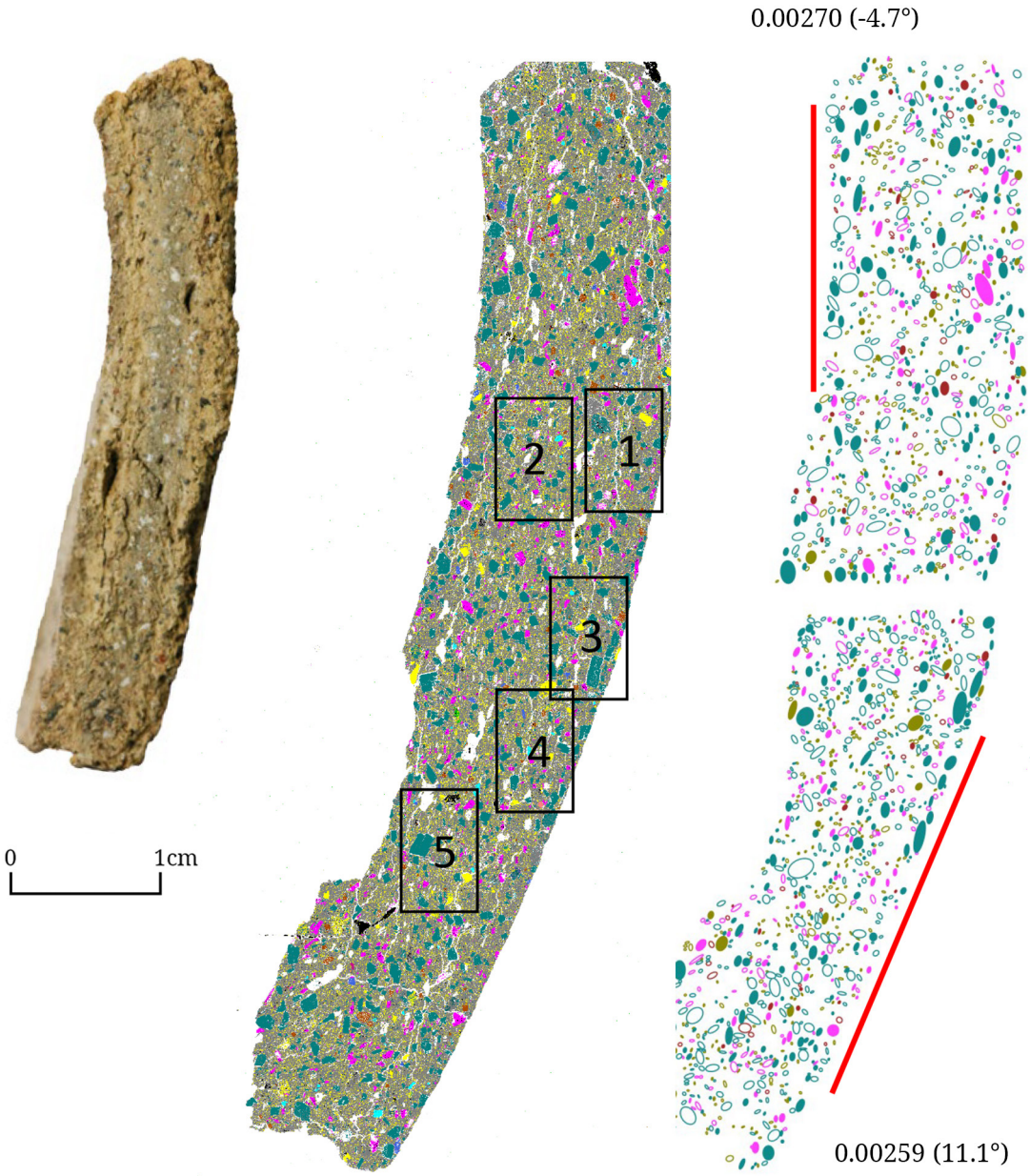

Fig. 28: Cross section, QEMSCAN map and ellipses for sample 132-1.

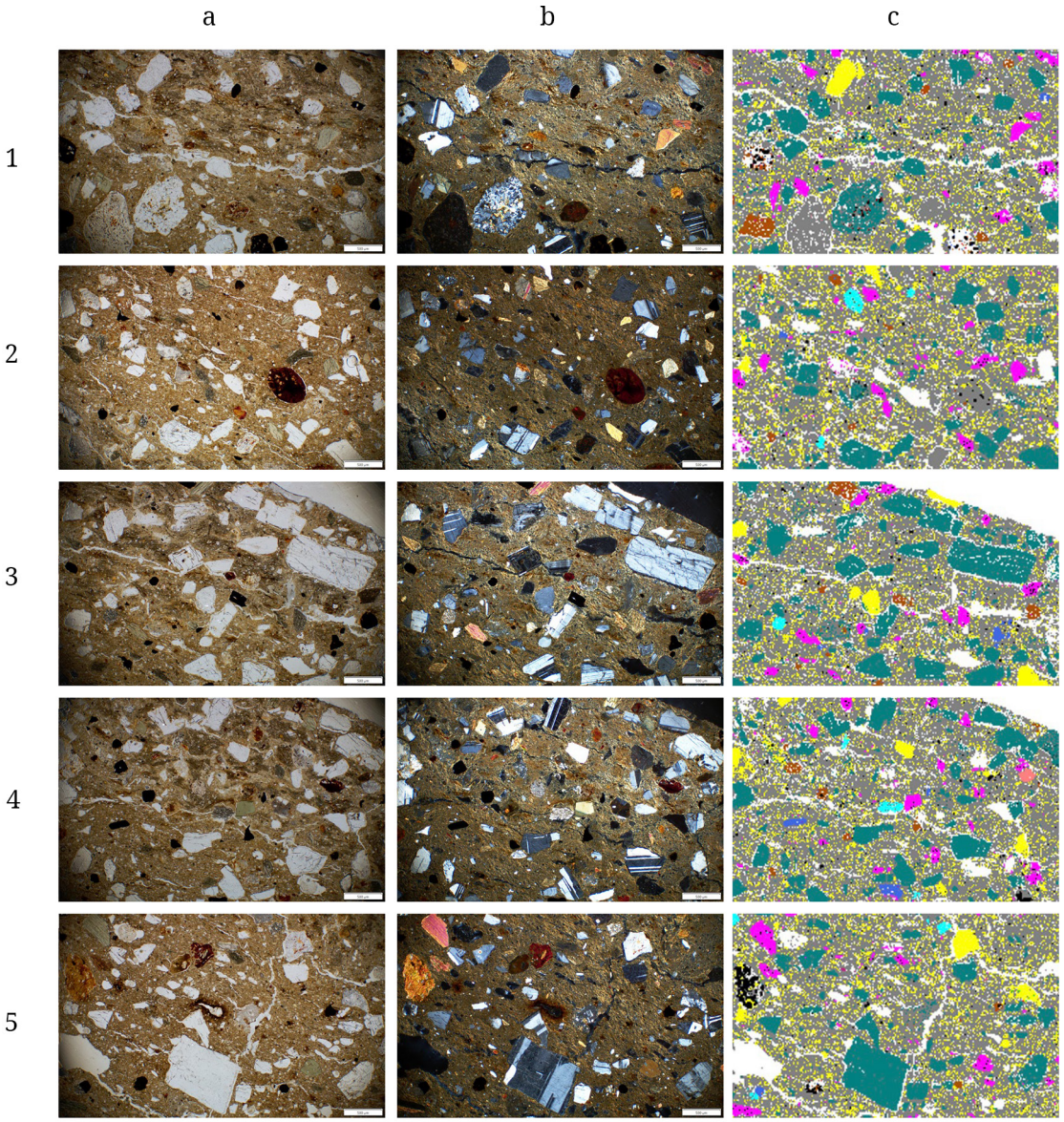

Fig. 29: Sample 132-1: Photomicrographs in plane- (left) and cross-polarised (centre) light, with the corresponding section of the QEMSCAN map on the right. The numbers correspond to the rectangles in Fig. 28.

Fig. 30: Cross section, QEMSCAN map and ellipses for sample 132-2.

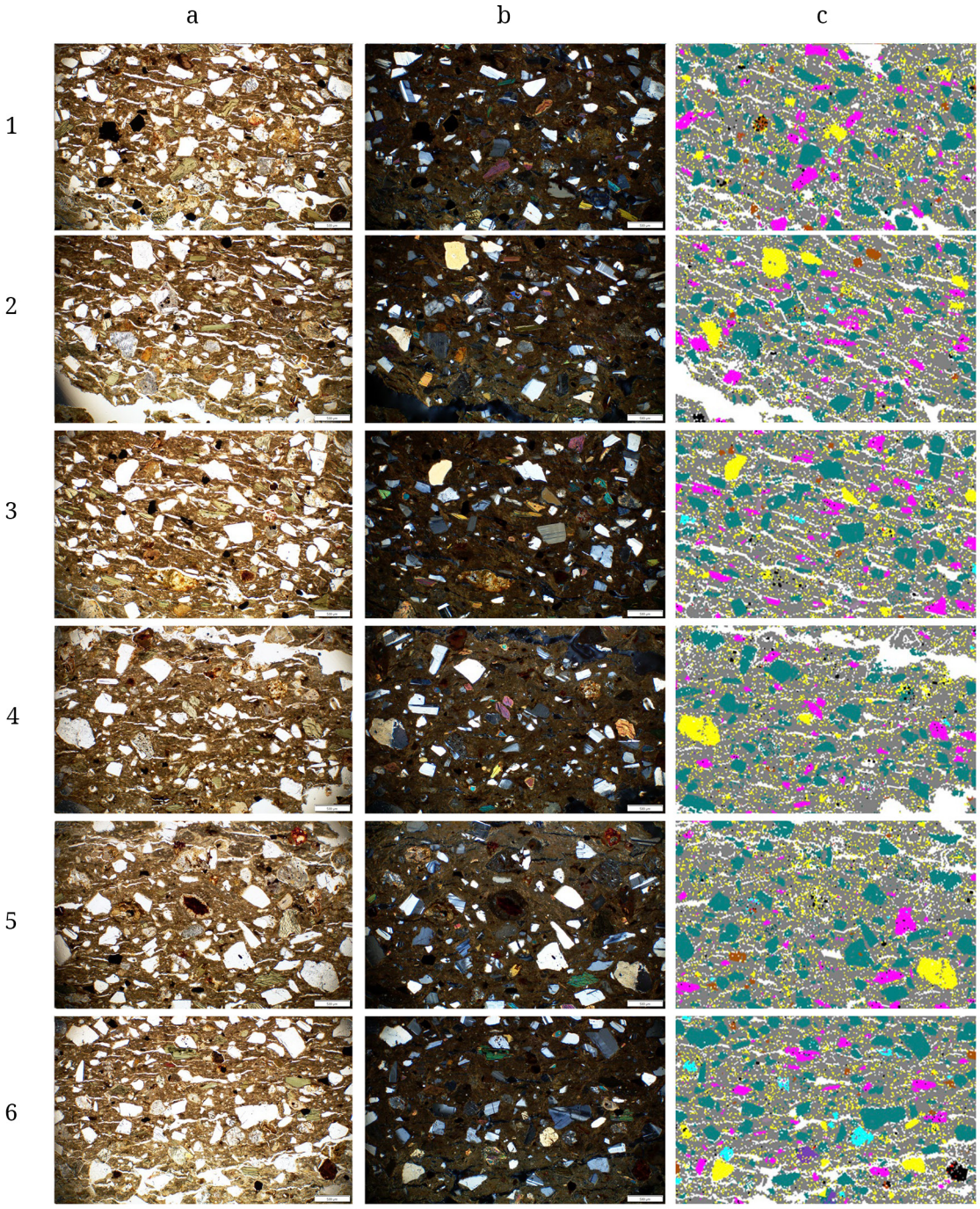

Fig. 31: Sample 132-2: Photomicrographs in plane- (left) and cross-polarised (centre) light, with the corresponding section of the QEMSCAN map on the right. The numbers correspond to the rectangles in Fig. 30.

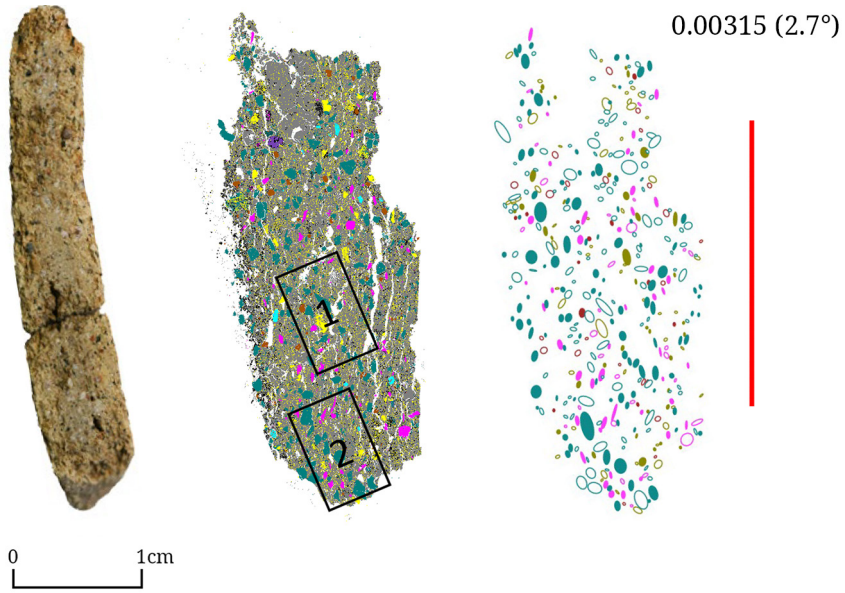

Fig. 32: Cross section, QEMSCAN map and ellipses for sample 147-2.

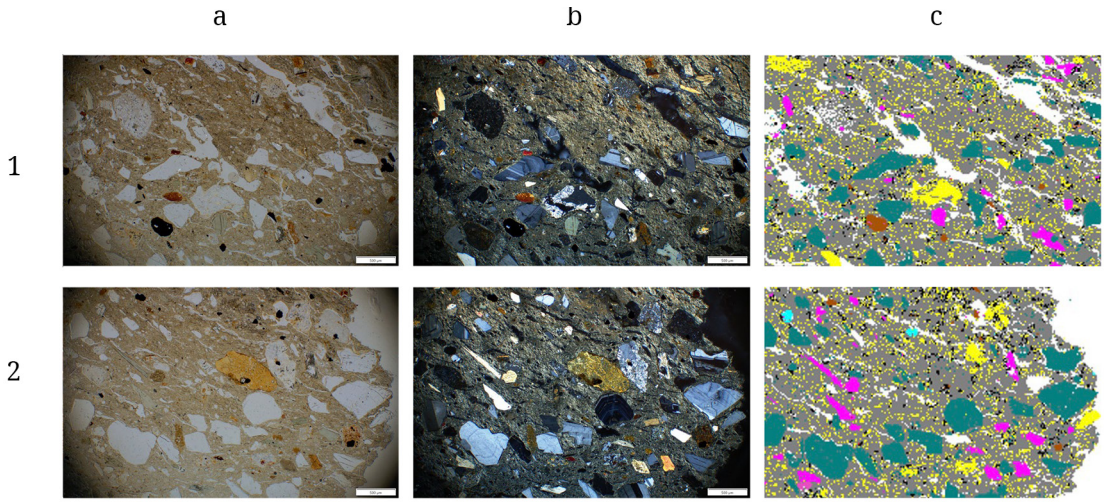

Fig. 33: Sample 147-2: Photomicrographs in plane- (left) and cross-polarised (centre) light, with the corresponding section of the QEMSCAN map on the right. The numbers correspond to the rectangles in Fig. 32.

References

Agostinelli, C. – Lund, U. 2022 R package 'circular': Circular Statistics.

Anggraeni, S. – Bellwood, T. – Piper, P. 2014 Neolithic foundations in the Karama valley, West Sulawesi, Indonesia. Antiquity, 88: 740–756.

Apandi, T. – Bachri, S. 1997 Peta Geologi Lembar Kotamobagu, 1 : 250000, Pusat Penelitian dan Pengembangan Geologi, Bandung.

Aprile, A. – Castellano, G. – Eramo, G. 2014 Combining image analysis and modular neural networks for classification of mineral inclusions and pores in archaeological potsherds. Journal of Archaeological Science 50: 262–272.

Aprile, A. – Castellano, G. – Eramo, G. 2019 Classification of mineral inclusions in ancient ceramics: comparing different modal analysis strategies. Archaeological and anthropological sciences 11: 2557–2567.

Azis, N. – Reepmeyer, C. – Clark, C. et al. 2018 Mansiri in North Sulawesi: A new dentate-stamped pottery site in Island Southeast Asia. In: O'Connor, S., Bulbeck, D. and Meyer, J. (Eds.) The archaeology of Sulawesi: Current research on the Pleistocene to the Historic Period. Canberra: ANU Press. Terra Australis 48, 191–205.

Berg, I. 2009 X-radiography of Knossian Bronze Age vessels: assessing our knowledge of primary forming techniques. The Annual of the British School at Athens 104, 137–173.

Berg, I. 2011 Exploring the chaineoperatoire of ceramics through X-radiography. In: Scarcella, S. (Ed.), Archaeological Ceramics: a Review of Current Research. Archaeopress, Oxford, pp. 57–63.

Berg, I. – Ambers, J. 2016 X-Radiography of archaeological ceramics. In: Hunt. A. (Ed.) The Oxford handbook of archaeological ceramic analysis. Oxford University Press.

Boggs, S. Jr. 2012 Principles of Sedimentology and Stratigraphy. 5th edition. Upper Saddle River, N. J.: Pearson Prentice Hall.

Bulbeck, F. D. – Nasruddin 2008 Recent insights on the chronology and ceramics of the Kalumpang site complex, South Sulawesi, Indonesia. BIPPA 22, 83–100.

Butcher, A. R. – Helms, T. A. – Gottlieb, G. Advances in the quantification of gold deportment by QemSCAN. Seventh Mill Operators' Conference, Kalgoorlie, Western Australia, 12–14 October, 2000. Melbourne, Vic: The Australasian Inst. of Mining & Metallurgy.

Carr, C. 1990 Advances in ceramic radiography and analysis: applications and potentials. Journal of Archaeological Science 17, 13–34.

Chia, S. 2003 The prehistory of Bukit Tengkorak as a major pottery making site in Southeast Asia. Sabah Museum Monograph 8.

Courty, M. A. – Roux, V. 1995 Identification of wheel throwing on the basis of ceramic surface features and microfabrics. Journal of Archaeological Science 22, 17–50.

Dal Sasso, G. – Maritan, L. – Salvatori, S. et al. 2014 Discriminating pottery production by image analysis: a case study of Mesolithic and Neolithic pottery from Al Khiday (Khartoum, Sudan). Journal of Archaeological Science 46: 125–143.

Denham, T. P. – Bronk Ramsey, C. – Specht, J. 2013 Dating the appearance of Lapita pottery in the Bismarck Archipelago and its dispersal to Remote Oceania. Archaeology in Oceania 47: 39–46.

Dickinson, W. R. 2006 Temper sands in prehistoric oceanian pottery: Geotectonics, sedimentology, petrography, provenance. Boulder, Colorado: The Geological Society of America. Vol. Special paper 406.

Edwards, T. – Groni, E. – Herries, A. I. R. et al. 2017 Visualising Scales of Process: Multi-Scalar Geoarchaeological Investigations of Microstratigraphy and Diagenesis at Hominin Bearing Sites in South African Karst. Journal of Archaeological Science 83: 1–11.

Eramo, G. – Aprile, A. – Muntoni, I. M. et al. 2014 Textural and morphometric analysis applied to Holocene pottery from Takarkori rock shelter (SW Libya, Central Sahara): a quantitative sedimentology approach. Archaeometry 56: 36–57.

Felicissimo, M. P. – Peixoto, J. L. – Bittencourt, C. et al. 2010 SEM, EPR and ToF-SIMS analyses applied to unravel the technology employed for pottery-making by precolonial Indian tribes from Pantanal, Brazil, Journal of Archaeological Science 37 (9), 2179–87.

Gaffney, D. – Summerhayes, G. R. – Ford, A. et al. 2015 Earliest pottery on New Guinea mainland reveals Austronesian influences in Highland environments 3000 years ago. PLoS One 10 (9), e0134497.

Goodall, W. R. 2008 Characterisation of mineralogy and gold deportment for complex tailings deposits using QEMSCAN®. Minerals Engineering 21: 518–523.

Goodall, W. R. – Scales, P. J. – Butcher, A. R. 2005 The use of QEMSCAN and diagnostic leaching in the characterisation of visible gold in complex ores. Minerals Engineering 18: 877–8P.

Gottlieb, P. – Wilkie, G. – Sutherland, D. et al. 2000 Using quantitative electron microscopy for process mineralogy applications. Journal of Mineralogy 52 (4): 24–25.

Gribble, C. D. – Hall, A. J. 1985 Optical Mineralogy: Principles and Practice. George Allen and Unwin, Hemel Hampstead, Hertfordshire, UK.

Hall, R. 2002 Cenozoic geological and plate tectonic evolution of SE Asia and the SW Pacific: computer-based reconstructions, model and animations, Journal of Asian Earth Sciences 20: 353–431.

Kavalieris, I. et al. 1992 Geological setting and styles of mineralization, north arm of Sulawesi, Indonesia, Journal of Southeast Asian Earth Sciences 7 (2/3): 113–129.

Knappett, C. D. – Pirrie, M. R. – Power, I. et al. 2011 Mineralogical analysis and provenancing of ancient ceramics using automated SEM-EDS analysis (QEMSCAN®): a pilot study on LB I pottery from Akrotiri, Thera. Journal of Archaeological Science 38: 219–232.

Kozatsas, J. – Kotsakis, K. – Sagris, D. et al. 2018 Inside out: Assessing pottery forming techniques with micro-CT scanning: an example from Middle Neolithic Thessaly. Journal of Archaeological Science 100: 102–119.

Leclerc, M. – Grono, E. – Bedford, B. et al. 2019 Assessment of the technology variability in decorated Lapita pottery from Teouma, Vanuatu, by petrography and LA-ICP-MS: implications for Lapita social organisation. Archaeological and Anthropological Sciences 11. 5257–5273.

MacKenzie, W. S. – Adams, A. E. 1994 A Colour Atlas of Rocks and Minerals in Thin Section. CRC Press, Boca Raton, Florida.

Martin, R. S. – Mather, T. A. – Pyle, D. M. et al. 2008 Composition-resolved size distributions of volcanic aerosols in the Mt. Etna plumes. Journal of Geophysical Research 113: D17211 (DOI: 10.1029/2007JD009648).

Mason, J. – Lin, E. – Grono, E. et al. 2022 QEMSCAN® analysis of clay-rich stratigraphy associated with early agricultural contexts at Kuk Swamp, Papua New Guinea. Journal of Archaeological Science: Reports. 103356 (DOI: doi.org/10.1016/j.jasrep.2022.103356).

Middleton, A. 2005 Ceramics. In: Lang, J., Middleton, A. (Eds.). Radiography of Cultural Material. Elsevier, Amsterdam, 76–95.

Nesse, W. D. 1991 Introduction to Optical Mineralogy [Second Edition]. Oxford University Press, New York.

Peterson, W. 1974 Summary Report of Two Archaeological Sites from North-Eastern Luzon. Archaeology & Physical Anthropology in Oceania, 9 (1): 26–35.

Pirrie, D. – Butcher, A. R. – Power, M. R. et al. 2004 Rapid quantitative mineral and phase analysis using automated scanning electron microscopy (QemSCAN); potential applications in forensic geoscience. Geological Society, London, Special Publications, 232: 123–136.

Pirrie, D. – Power, M. R. – Rollinson, G. K. et al. 2009 Automated SEM-EDS (QEMSCAN®) mineral analysis in forensic soil investigations: testing instrumental reproducibility. In Ritz, R., Dawson, L, Miller, D. (Eds.), Criminal and Environmental soil forensics. 411–430.

Prossor, L. – Denham, T. – Brink, F. et al. 2022 The microstratigraphic investigation of hearth features at Lake Mungo, Australia. Journal of Archaeological Science: Reports. 46. 103711 (DOI: doi.org/10.1016/j.jasrep.2022.103711).

Quinn, P. S. 2013 Ceramic Petrography: The interepretation of archaeological pottery & related artefacts in thin section. Oxford: Archaeopress.

Reedy, C. L. 2008 Thin-section petrography of stone and ceramic cultural materials. Archetype Publications, London.

Reedy, C. L. – Anderson, J. – Reedy, T. J. et al. 2014 Image analysis in quantitative particle studies of archaeological ceramic thin sections. Advances in archaeological practice 2 (4): 252–268.

Rye, O. S. 1977 Pottery manufacturing techniques: X-ray studies. Archaeometry 19, 205–211.

Rye, O. S. 1981 Pottery technology: principles and reconstruction. Taraxacum, Washington D.C.

Sanger, M. C. 2016 Investigating pottery vessel manufacturing techniques using radiographic imaging and computed tomography: studies from the Late Archaic American Southeast. Journal of Archaeological Science: Report 9, 586–598.

Schindelin, J. – Arganda-Carreras, I. – Frise, E. et al. 2012 Fiji: an open-source platform for biological-image analysis. Nat. Methods 9, 676–682.

Šegvić, B. – Süssenberger, A. – Ugarković, M. et al. 2014 Mineralogy and cultural heritage – introducing QEMSCAN® automated technology to the study of ancient artefacts. In: 12th Swiss Geoscience Meeting, 21–22 November 2014, Fribourg (Switzerland), 1–2.

Šegvić, B. – Ugarković, M. – Süssenberger, A. et al. 2016 Compositional properties and provenance of Hellenistic pottery from the Necropolis of Issawith evidences on the cross-Adriatic and the Mediterranean-scale trade. Mediterranean Archaeology and Archaeometry 16 (1): 23–52.

Simanjuntak, T. – Soejono, R. P. et al. 2006 Archaeology: Indonesian Perspective: R.P. Soejono's festschrift. Indonesian Institute of Sciences, International Center for Prehistoric and Austronesian Studies, Jakarta.

Specht, J. – Denham, T. P. – Goff, J. et al. 2014 Deconstruction the Lapita Cultural Complex in the Bismarck Archipelago. Journal of Archaeological Research 22: 89–140.

Swete-Kelly, M. C. 2017 Early Pottery in Island Southeast Asia. In: Habu, J., Lape, P.V., Olsen, J.W. (Eds.) Handbook of East and Southeast Asian Archaeology. Springer, New York, NY. 397–418.

Thér, R. 2016 Identification of pottery-forming techniques using quantitative analysis of the orientation of inclusions and voids in thin sections. Archaeometry 58, 222–238.

Tucker, M. E. 2001 Sedimentary petrology. Oxford: Blackwell Science Ltd.

Van Leeuwen, T. – Pieters, P. E. 2011 Mineral Deposits of Sulawesi. In: The Sulawesi Mineral Resources 2011 Seminar MGEI-IAGI. Masyarakat Geologi Ekonomi Indonesia (MGEI)-Ikatan Ahli Geologi Indonesia (IAGI). Manado, Indonesia. 1–130.

Ward, I. – Veth, P. – Prossor, L. et al. 2017 50,000 years of archaeological site stratigraphy and micromorphology in Boodie Cave, Barrow Island, Western Australia. Journal of Archaeological Science: Report 15. 344–369.

Whitbread, I. K. 1996a A proposal for the systematic description of thin sections. Towards the study of ancient ceramic technology. In: Maniatis, Y. (Ed.), Archaeometry: Proceedings of the 25th International Symposium. Elsevier, Amsterdam, 127–138.

Whitbread, I. K. 1996b Detection and interpretation of preferred orientation in ceramic thin sections. In: Stratis, I., Vavelidis, M., Kotsakis, K., Tsokas, G., Tsoukala, E. (Eds.), Archaeometrical and Archaeological Research in Macedonia and Thrace. Proceedings of the 2nd Symposium, Thessaloniki 26–28 May 1993. Hellenic Archaeometrical Society, Thessaloniki. 413–425.

Wickham, H. 2016 ggplot2: Elegant Graphics for Data Analysis. Springer-Verlag, New York.

Winter, O. 2015 Colonisation of the Mariana Islands: Affinities and differences between ISEA and Pacific cultures in the 1st millennium BC. Unpublished PhD thesis, ANU.

SOURCE OF ILLUSTRATIONS

Cover: K. Hardy
Fig. 1: C. Reepmeyer
Fig. 2: M. Leclerc
Fig. 3: M. Leclerc
Fig. 4: M. Leclerc
Fig. 5: U. Troitzsch
Fig. 6: M. Leclerc
Fig. 7: K. Hardy
Fig. 8: K. Hardy
Fig. 9: K. Hardy
Fig. 10: K. Hardy
Fig. 11: K. Hardy
Fig. 12: K. Hardy
Fig. 13: K. Hardy
Fig. 14: K. Hardy / M. Leclerc
Fig. 15: K. Hardy
Fig. 16: K. Hardy / M. Leclerc
Fig. 17: K. Hardy
Fig. 18: K. Hardy / M. Leclerc
Fig. 19: K. Hardy
Fig. 20: K. Hardy / M. Leclerc
Fig. 21: K. Hardy
Fig. 22: K. Hardy / M. Leclerc
Fig. 23: K. Hardy
Fig. 24: K. Hardy / M. Leclerc
Fig. 25: K. Hardy
Fig. 26: K. Hardy / M. Leclerc
Fig. 27: K. Hardy
Fig. 28: K. Hardy / M. Leclerc
Fig. 29: K. Hardy
Fig. 30: K. Hardy / M. Leclerc
Fig. 31: K. Hardy
Fig. 32: K. Hardy / M. Leclerc
Fig. 33: K. Hardy

AUTHORS

Dr. Mathieu Leclerc
Australian National University
Canberra ACT 2601
Australia
mathieu.leclerc@anu.edu.au
https://orcid.org/0000-0003-1093-802X
https://ror.org/019wvm592

Kristine Hardy
Australian National University
Canberra ACT 2601
Australia
Kristine.Hardy@anu.edu.au
https://orcid.org/0000-0003-1660-4477
https://ror.org/019wvm592

Dr. Elle Grono
Australian National University
Canberra ACT 2601
Australia
https://orcid.org/0000-0002-3607-6686
https://ror.org/019wvm592

Dr. Tse Siang Lim
Australian National University
Canberra ACT 2601
Australia
https://orcid.org/0000-0003-3127-9932
https://ror.org/019wvm592

Dr. Ulrike Troitzsch
Australian National University
Canberra ACT 2601
Australia
Ulrike.Troitzsch@anu.edu.au
https://orcid.org/0000-0001-6317-8509
https://ror.org/019wvm592

Dr. Frank Brink
Australian National University
Canberra ACT 2601
Australia
frank.brink@anu.edu.au
https://ror.org/019wvm592

Prof. Dr. Geoffrey Clark
Australian National University
Canberra ACT 2601
Australia
geoffrey.clark@anu.edu.au
https://orcid.org/0000-0002-9055-655X
https://ror.org/019wvm592

Dr. Daud Tanudirjo
Universitas Gadjah Mada
Yogyakarta 55281
Indonesia
daud.tanudirjo@ugm.ac.id
https://orcid.org/0000-0003-3002-4161
https://ror.org/03ke6d638

Nazrullah Azis
Regional Agency for Archaeological Research in North Sulawesi Province
Sulawesi
Indonesia
ulla@archaeologist.com

Dr. Christian Reepmeyer
Commission for Archaeology of Non-European Cultures (DAI) / College of Arts, Society and Education (JCU)
Dürenstraße 35–37
53173 Bonn
Germany
Christian.Reepmeyer@dainst.de
https://orcid.org/0000-0002-3257-0898
https://ror.org/02rspp784

METADATA

Titel/*Title*: Automated analysis of pottery by QEM-EDS: A case study from Mansiri, Sulawesi

Band/*Issue*: 23/3

Bitte zitieren Sie diesen Beitrag folgenderweise/*Please cite the article as follows*: M. Leclerc – K. Hardy – E. Grono – T. Siang Lim – U. Troitzsch – F. Brink – G. Clark – D. Tanudirjo – N. Azis – C. Reepmeyer, Automated analysis of pottery by QEM-EDS: A case study from Mansiri, Sulawesi, JoGA 2023/3, § 1–49, 50–93, https://doi.org/10.34780//b92n-4tna

Online veröffentlicht am/*Online published on*: 20.06.2023

DOI: https://doi.org/10.34780/b92n-4tna

Schlagwörter/*Keywords*: Automated analysis of pottery by QEM-EDS: A case study from Mansiri, Sulawesi

Bibliographischer Datensatz/*Bibliographic reference*: https://zenon.dainst.org/Record/003042644